Geol. Mag. **143** (*6*), *2006, pp. 777–796.* © *2006 Cambridge University Press*
doi:10.1017/S0016756806002597 *Printed in the United Kingdom*

A new stratigraphy for the Latady Basin, Antarctic Peninsula: Part 1, Ellsworth Land Volcanic Group

M. A. HUNTER*†, T. R. RILEY*, D. J. CANTRILL‡, M. J. FLOWERDEW* & I. L. MILLAR§

*British Antarctic Survey, Natural Environment Research Council, High Cross, Madingley Road, Cambridge CB3 0ET, UK
‡Swedish Museum of Natural History, Department of Palaeobotany, Box 50007, Stockholm 104 05, Sweden
§NERC isotope Geosciences Laboratory, Keyworth, Nottingham, NG12 5GG, UK

(*Received* 22 September 2005; *accepted* 4 January 2006)

Abstract – The Jurassic Mount Poster Formation of eastern Ellsworth Land, southern Antarctic Peninsula, comprises silicic ignimbrites related to intracontinental rifting of Gondwana. The identification of less voluminous basaltic and sedimentary facies marginal to the silicic deposits has led to a reclassification of the volcanic units into the Ellsworth Land Volcanic Group. This is formally subdivided into two formations: the Mount Poster Formation (silicic ignimbrites), and the Sweeney Formation (basaltic and sedimentary facies). The Mount Poster Formation rhyolites are an intracaldera sequence greater than 1 km in thickness. The basaltic and sedimentary facies of the Sweeney Formation are consistent with deposition in a terrestrial setting into, or close to, water. The geochemistry of the Mount Poster Formation is consistent with derivation of the intracaldera rhyolites from a long-lived, upper crustal magma chamber. The basalts of the Sweeney Formation are intermediate between asthenosphere- and lithosphere-derived magmas, with little or no subduction-modified component. The basalt could represent a rare erupted part of the basaltic underplate that acted as the heat source for local generation of the rhyolites. U–Pb ion microprobe zircon geochronology of samples from the Mount Poster Formation yield an average eruption age of 183.4 ± 1.4 Ma. Analysis of detrital zircons from a Sweeney Formation sandstone suggest a maximum age of deposition of 183 ± 4 Ma and the two formations are considered coeval. In addition, these ages are coincident with eruption of the Karoo-Ferrar Igneous Province in southern Africa and East Antarctica. Our interpretation of the Ellsworth Land Volcanic Group is consistent with the model that the Jurassic volcanism of Patagonia and the Antarctic Peninsula took place in response to intracontinental extension driven by arrival of a plume in that area.

Keywords: geochemistry, crustal contamination, rhyolite, basalt, Antarctica, U–Pb.

1. Introduction

With the exception of Cenozoic volcanic rocks associated with the slowing and cessation of subduction, Thomson & Pankhurst (1983) assigned all Jurassic–Cenozoic volcanic rocks in the Antarctic Peninsula to the Antarctic Peninsula Volcanic Group, which was regarded as the product of magmatic arc volcanism at the palaeo-Pacific margin of Gondwana (Storey & Garrett, 1985). Many of the igneous rocks exposed on the western side of the Antarctic Peninsula are Cretaceous in age and have intermediate compositions. However, the eastern Peninsula is dominated by thick deposits (> 1 km) of largely silicic volcanic (and plutonic) rocks, typically of Early and Middle Jurassic age (Pankhurst *et al.* 2000). Middle Jurassic volcanic units in eastern Graham Land were assigned to the Mapple Formation by Riley & Leat (1999), while Early Jurassic volcanic rocks in Palmer Land and Ellsworth Land were assigned to the Brennecke (Wever & Storey, 1992) and Mount Poster (Rowley, Schmidt & Williams, 1982) formations, respectively. More recently, Pankhurst *et al.* (2000) suggested that Early Jurassic silicic volcanism was generated in response to basaltic underplating associated with the arrival of a mantle plume under South Africa/East Antarctica *c.* 183 million years ago. By the Late Jurassic, Antarctic Peninsula volcanic rocks became increasingly intermediate in their composition with an increasing subduction-modified component. By Cretaceous times, production of magma was wholly subduction related, leading to the generation of the Andean–Antarctic Peninsula arc.

Initial extension of the Gondwana supercontinent took place during the Early Jurassic (Storey *et al.* 1992), and the volcanic and sedimentary facies deposited in basins developing at this time contain a unique record of supercontinent rifting in the evolution of their depositional environments, geochemistry and magma petrogenesis.

This study focuses on the Early Jurassic volcanic rocks of the southern Antarctic Peninsula where they crop out within the Latady Basin, eastern Ellsworth Land (Fig. 1). The Latady Basin contains a series of Early Jurassic (see Section 3; Fanning & Laudon,

†Author for correspondence: MAHU@bas.ac.uk

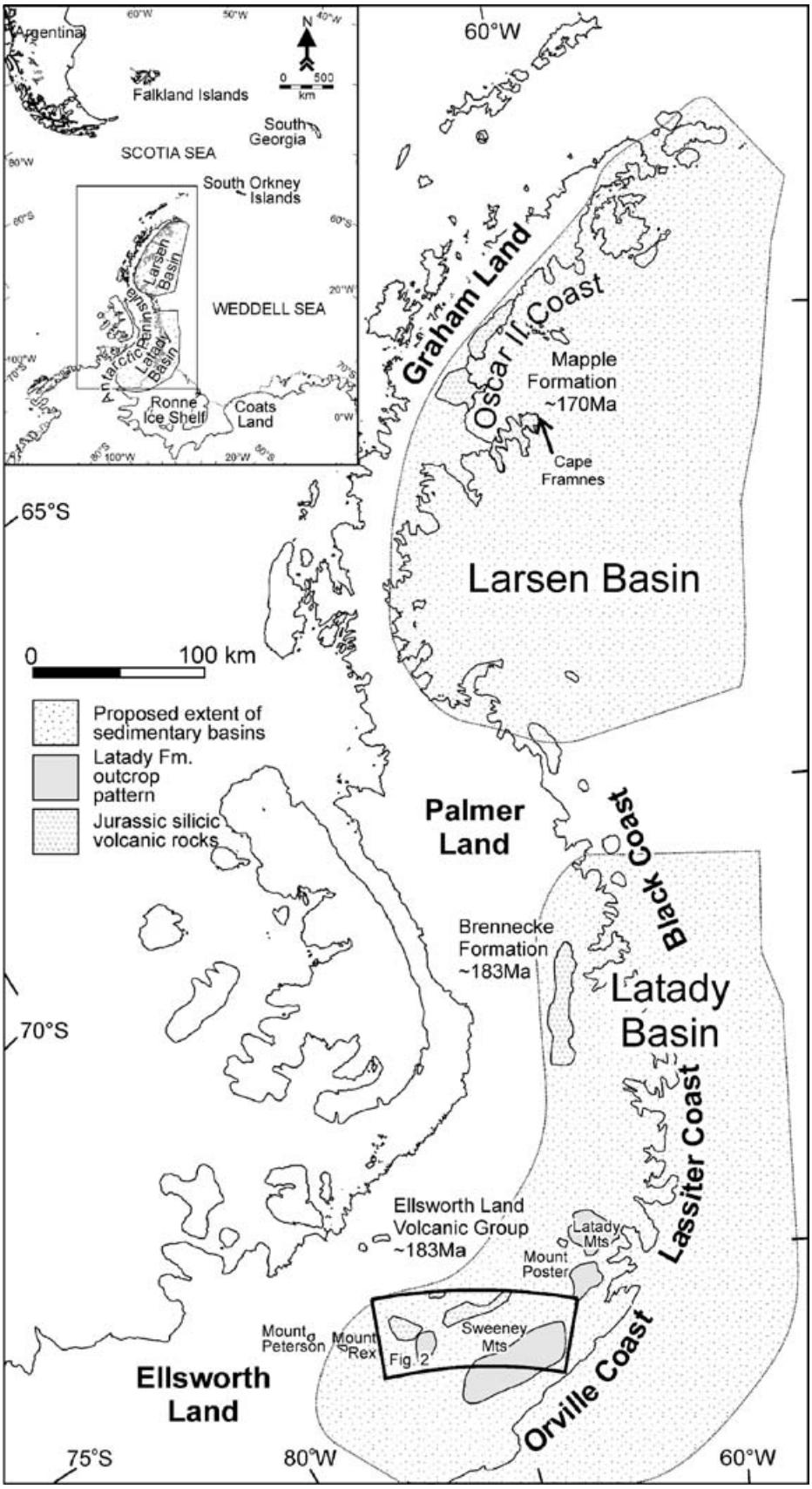

Figure 1. Map of the Antarctic Peninsula showing the distribution of the Latady and Larsen basins and their proposed extent based on geophysical and geological data. The extent of Jurassic-age silicic volcanic rocks is shown, as is the outcrop pattern of the Latady Formation. The ages of the silicic volcanic Mapple and Brennecke formations are taken from Pankhurst *et al.* (2000), and the age of the Ellsworth Land Volcanic Group is from this study.

https://doi.org/10.1017/S0016756806002597 Published online by Cambridge University Press

1999), largely silicic volcanic rocks assigned to the Mount Poster Formation (Rowley, Schmidt & Williams, 1982), overlain by several kilometres of Jurassic–Early Cretaceous marine and terrestrial sediments of the Latady Group (described in Hunter & Cantrill, 2006, this issue). As originally defined, all silicic volcanic rocks in the area are assigned to the Mount Poster Formation. However, the eruptive component is bimodal, with small but significant amounts of basaltic lava associated with sedimentary facies located at the margins of the silicic deposits. As a result, the volcanic suite has been raised to Group status, the Ellsworth Land Volcanic Group, with two formations: the Mount Poster Formation (silicic volcanic rocks) and the Sweeney Formation (basaltic lava and sedimentary facies). Jurassic volcanism in the eastern Antarctic Peninsula and southern South America is dominated by rhyolite with very few occurrences of basalt (Bryan *et al.* 2002). The volumetrically small basalt exposures within the Latady Basin are very important for understanding magma generation during supercontinental break-up. We also present new U–Pb zircon geochronology for the Ellsworth Land Volcanic Group and a brief discussion of the geochemistry of the rhyolites and basalts.

2. Ellsworth Land Volcanic Group

The Mount Poster Formation, as defined by Rowley, Schmidt & Williams (1982), included exposures at Mount Poster, west of the Latady Mountains (Fig. 1), and their continuation to the volcanic outcrops of the Orville Coast (Fig. 1). They described 600 m of silicic volcanic material overlying and interbedded with subaerial, fluvial or lacustrine sediments attributed to the Latady Formation (Williams *et al.* 1972). However, the exposure at Mount Poster is strongly deformed and metamorphosed, making stratigraphy and geochemical analysis difficult. Riley & Leat (1999) described the Mount Poster Formation from the less-deformed exposures in eastern Ellsworth Land as predominantly intracaldera dacitic to rhyodacitic pyroclasitc rocks and lava flows with minor extracaldera rocks dominated by basaltic compositions interbedded with sedimentary rocks, the first mention of any basaltic material in the succession. They suggested that the formation is about 500 m thick, locally reaching up to 1 km (Riley & Leat, 1999). Fanning & Laudon (1999) dated (U–Pb, zircon) three samples from the Mount Poster Formation, which yielded ages of 189 ± 3 Ma (Sweeney Mountains), 188 ± 3 Ma (Mount Peterson) and 167 ± 3 Ma (Mount Rex). The two older ages of the Mount Poster Formation are marginally older, but within error of the nearby Brennecke Formation (*c.* 184 ± 2 Ma: Pankhurst *et al.* 2000), which is believed to be part of the same Early Jurassic event. The 167 ± 3 Ma age for Mount Rex coincides with the age of the Mapple Formation in the northern part of the Antarctic Peninsula (Pankhurst *et al.* 2000). The two Early Jurassic ages, coupled with a Middle and Late Jurassic deposition of the Latady Formation (e.g. Quilty, 1972, 1977, 1983; Thomson, 1983), place the volcanic rocks at the base of the Latady Basin stratigraphy. A direct contact between the volcanic rocks and the Latady Group is not exposed, but the presence of an air fall tuff (Witte Nunataks Formation: Hunter, Riley & Millar, 2004) interbedded with sandstone and mudstone of the Latady Formation indicates that volcanism continued during deposition of the Latady Group as defined by Hunter & Cantrill (2006, this issue).

2.a. Mount Poster Formation

Nomenclature. We have retained the name of the original formation for the silicic ignimbrites as it is well established in the literature, and apart from removing the basaltic lava and sedimentary facies from the formation, the lithologies assigned to this formation remain essentially unchanged.

Type section. The formation was originally defined from a 3 km ridge section at Mount Poster (Rowley, Schmidt & Williams, 1982). However, this area has experienced higher degrees of deformation and metamorphism compared with Ellsworth Land exposures further west and south. This section is therefore unlikely to be representative of the formation in its wider context. Although it is difficult to correlate the volcanic units due to within-flow facies variations and minor faulting, a probable observed thickness of 1000 m is estimated in the Sweeney Mountains region. Given the difficulties in correlating units, defining a type section for the Mount Poster Formation is not only difficult but would be misleading.

Distribution, thickness and boundaries. As well as Mount Poster itself, the majority of the high peaks in the Sweeney Mountains, Henry, Lyon and Cheeks nunataks and Mount Wasilewski are composed of silicic ignimbrite (Fig. 2). No upper boundary is seen and, where present, the contact with the Sweeney Formation is faulted or intruded by dykes. The unit reaches a minimum of $\sim$ 500 m, although a thickness of at least 2 km has been estimated for the entire formation (Rowley, Schmidt & Williams, 1982).

Lithology. The formation is dominated by feldspar-phyric, fine-grained, poorly welded, crystal-rich, silicic ignimbrite that weathers blue/grey, green or purple, with minor tuffaceous units and rare lava flows. Large clusters (up to 8 cm diameter) of feldspar characterize the ignimbrite at many localities and give the rocks a characteristic apparent porphyritic texture. Lithic-rich units (Fig. 3a) are dominated by blocks of ignimbritic material and common, rounded quartzite/vein quartz clasts. Small flecks or clasts of red mudstone are

https://doi.org/10.1017/S0016756806002597 Published online by Cambridge University Press

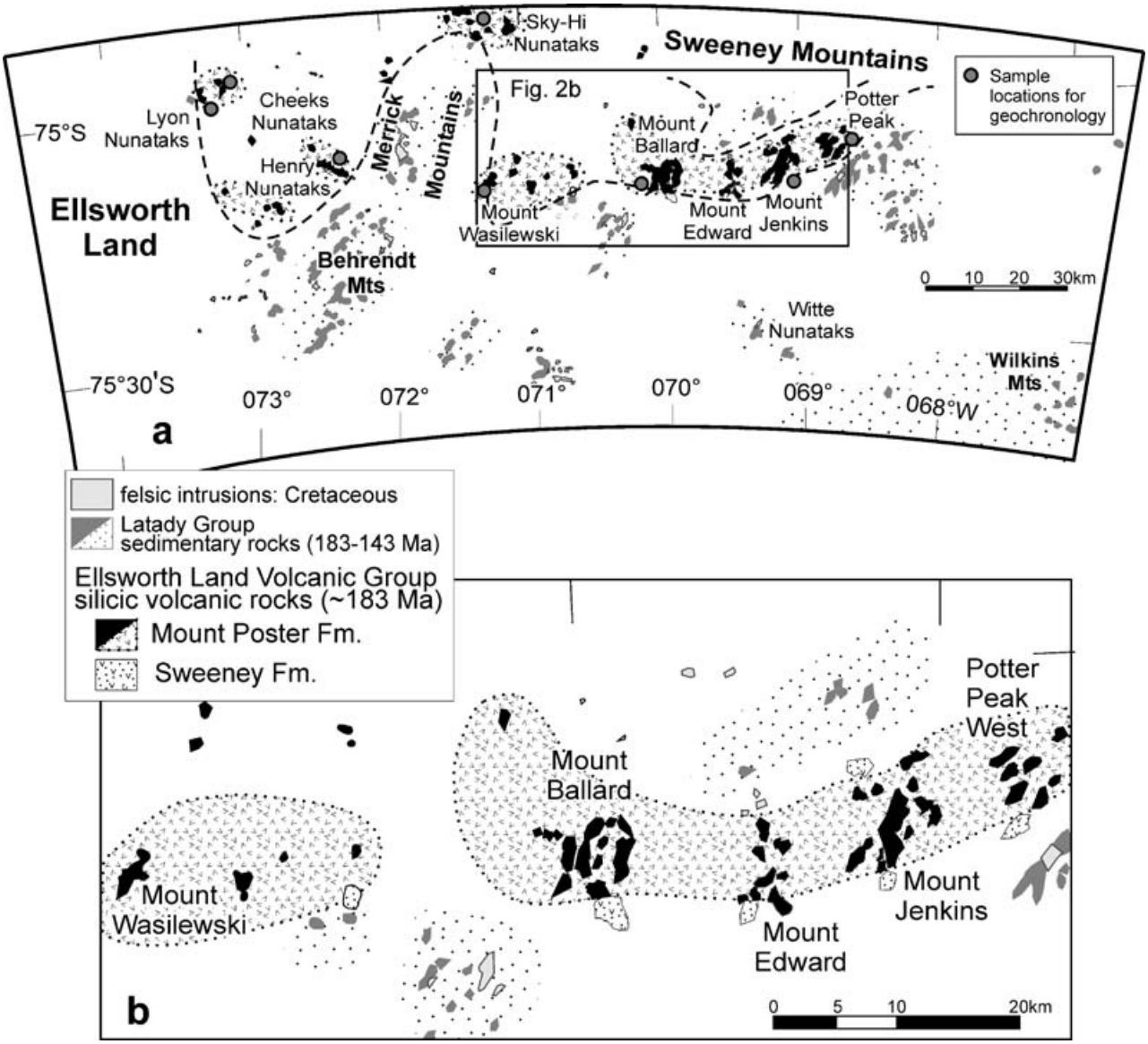

Figure 2. (a) Map of the study area showing the distribution of the Latady Group and the Ellsworth Land Volcanic Subgroup. The dashed line represents the possible contact between the two units. (b) Inset map showing detail of the Mount Poster and Sweeney formations in the Sweeney Mountains and at Mount Wasilewski. The probable extent of the Mount Poster Formation is enclosed by the dotted line.

ubiquitous but richer in some outcrops than others. Finely disseminated, variably weathered pyrite accounts for much of the difference in colour between outcrops. Late-stage epidote and quartz veining are common and can contain hornblende or iron oxide crystals. In strongly welded units, fiamme (Fig. 3b) are only weakly discernible, but poorly welded ignimbrites contain oblate, crystal-rich pumices (Fig. 3c), which account for up to 20 % of the rock. At one locality, strongly welded ignimbrite units, with pumice flattening ratios of up to 10:1, occur in association with rheomorphic ignimbrites that have well-defined parataxitic texture.

Depositional environment. An intracaldera setting for the formation is suggested by the lithological homogeneity and dense welding of most of the ignimbrites, the thickness of the succession, the pervasive low-grade alteration and faulting, and dyke emplacement at the putative caldera margins (Riley *et al.* 2001). Such features are characteristic of intracaldera ignimbrite-dominated successions from the western contiguous United States (Lipman, 1984) and Alaska (Bacon, Foster & Smith, 1990). Lithic- and pumice-rich horizons may mark separate eruptive events. The rhyolites are interpreted to be sourced from several separate centres, which may have resulted in a sequence of overlapping or nested calderas forming the present-day elongate outcrop pattern. Field evidence to support a pattern of overlapping calderas is limited, although faulting and dyke emplacement at the contact with the presumably contemporaneous Sweeney Formation probably mark the

https://doi.org/10.1017/S0016756806002597 Published online by Cambridge University Press

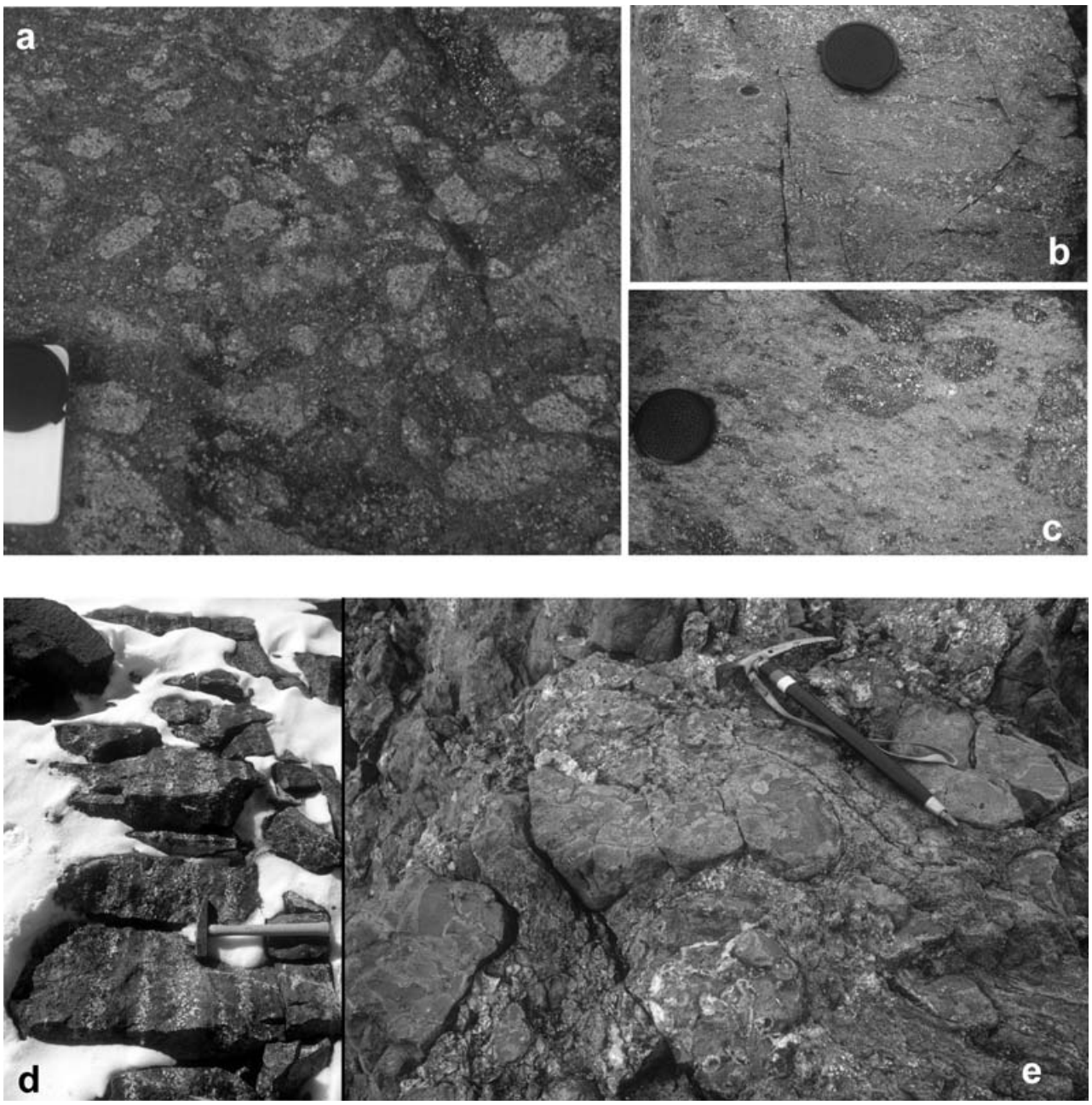

Figure 3. (a) Lithic-rich Mount Poster Formation ignimbrite unit from R.7104, Mount Jenkins. Lens cap is 52 mm diameter. (b) Flattened pumice (fiamme) in Mount Poster Formation ignimbrite from SE Mount Jenkins. Lens cap is 52 mm diameter. (c) Oblate, crystal-rich pumice in Mount Poster Formation ignimbrite from R.7108, Potter Peak. Lens cap is 52 mm diameter. (d) Linear pattern in amygdaloidal basalts of the Sweeney Formation, southern Mount Jenkins. Length of hammer is 35 cm. (e) Pillow basalts of the Sweeney Formation, northern Mount Jenkins. Length of ice axe is 60 cm.

caldera margin, and rare high aspect-ratio extracaldera ignimbrites are interpreted to represent distal outflow units.

Age. New ion-microprobe U–Pb analyses of zircon from the intracaldera ignimbrites date these deposits at 183.4 ± 1.4 Ma, contemporaneous with the plume-related Karoo and Ferrar provinces in southern Africa and the Transantarctic Mountains (see Section 3; Riley & Knight, 2001). When combined with pre vious Early Jurassic ages from the intracaldera facies (*c.* 188 Ma: Fanning & Laudon, 1999), these data suggest that the onset of volcanism either marginally preceded or was coeval with earliest sedimentation in the Sweeney Formation (see Section 3).

2. b. Sweeney Formation

Previous authors assigned these sedimentary facies to the Latady Formation and the volcanic facies to the Mount Poster Formation (Laudon *et al.* 1983).

https://doi.org/10.1017/S0016756806002597 Published online by Cambridge University Press

However, no lacustrine facies are found in the Latady Group (Hunter & Cantrill, 2006, this issue), and the Mount Poster Formation (Rowley, Schimdt & Williams, 1982) was originally defined from the silicic intracaldera deposits at Mount Poster where there is no outcrop of basaltic material. For these reasons we assign these extracaldera facies, both volcanic and sedimentary, to a separate formation: the Sweeney Formation, within the Ellsworth Land Volcanic Group.

Nomenclature. The Sweeney Formation is named after the Sweeney Mountains where it comprises many of the peripheral nunataks, both to the north and south of the main range (Fig. 2).

Type section. The type section is designated from the most southerly ridge of Potter Peak West (Figs 2, 3). The ridge is 2.25 km long and underlain by volcanic and fine-grained sedimentary facies typical of this formation.

Distribution, thickness and boundaries. The formation underlies the most southerly ridges of Potter Peak West, Mount Jenkins, Mount Edward and Mount Ballard, a ridge to the northwest of the peak of Mount Jenkins and an isolated flat-lying outcrop to the east of Mount Wasilewski (Fig. 2). No basal contact or contact with the Latady Group was observed and, where present, contact with the proximal Mount Poster Formation is faulted or intruded (Riley & Leat, 1999). The greatest thickness of the Sweeney Formation crops out at the type section where ~ 300 m of black finely laminated mudstone and sandstone (Fig. 4) are interbedded with at least 1000 m of basaltic lava and silicic pyroclastic (distal ignimbrite) deposits. Elsewhere the sedimentary facies are more typically tens of metres thick (Fig. 4). The ridges south and southeast of Mount Ballard are underlain by at least 600 m of predominantly basaltic volcanic facies with minor fine-grained sediment.

Lithology. The formation consists of abundant volcanic with less voluminous fine-grained sedimentary facies. The most distinctive facies is amygdaloidal basalt, with a dark green or black fine-grained matrix, and cream or white amygdales that form lines, possibly defining individual flows or multiple crusts generated during flow development (Fig. 3d), akin to the Kamenev Formation of the Black Coast (Fig. 1) described by Storey *et al.* (1987). Amygdales vary in quantity and size between flows, from less than a centimetre up to 6 cm or more. Many amygdales are elongate. Other basaltic flows can be aphyric or phyric with small phenocrysts of feldspar and clinopyroxene. Rarely, flows can be vesicular, and minor pillow basalt crops out at Mount Jenkins and Mount Ballard (Fig. 3e). Some pillows are set in a hyaloclastite matrix and a hyaloclastic breccia was noted to the south of Mount Jenkins. The remainder of the volcanic facies are either pyroclastic, including ash-rich and pebble-rich ignimbritic units, or finely bedded ash-fall horizons and graded lapilli tuffs, sometimes with cross-ripple lamination consistent with deposition into, or reworking by, water. Sometimes these well-bedded units show convoluted bedding.

The sedimentary sections are dominated by very dark coloured, red weathering, fine-grained sandstone and mudstone, deposited in millimetre-scale beds (Fig. 5a), either as sandstone/mudstone pairs, or graded in 0.5–1 cm scale beds capped by thin drapes of black claystone. Bedding is generally planar or ripple cross-laminated, but in many instances can be convoluted over a distance of 5–10 cm (Fig. 5b). Subsequent beds drape the syn-sedimentary structures until planar bedding is resumed (Fig. 5b). Plant material is found throughout the sedimentary facies but is not abundant. At Potter Peak West, silicified wood, *Brachyphyllum* sp. and *Elatocladus confertus* shoots, and cross-cutting roots up to 3 cm in diameter are consistent with the growth of conifers between eruptive phases (Fig. 6a–c). Elsewhere, mudstone contains poorly preserved isolated plant remains, and ignimbrite and lava flow tops can include some quite sizeable wood debris. Beds of 2–4 m thickness of orange weathering, grey medium/fine- to fine-grained sandstone are the only other significant lithology. They are normally planar bedded, sometimes picked out by very thin siltstone partings, although weathering often makes them appear structureless.

Depositional environment. The volcanic and sedimentary facies are interbedded and contemporaneous. Sedimentary beds at the contact with volcanic facies often show signs of baking or disruption: red mudstone draping basaltic flows, turning black away from the contact, or disrupted and eroded bedding underlying lava bodies. Many of the well-bedded sedimentary facies and finer ash-fall horizons show convoluted bedding, almost certainly generated as a result of nearby eruptions, or associated earth tremors. The sedimentary facies are predominantly well-sorted, rhythmically bedded sandstone and siltstone, with small fining-up sequences and ripple-laminated horizons. The presence of root horizons and fossil tree debris is consistent with shallow water, and the lack of any other fossiliferous material or bioturbation suggests that the sediments were deposited in fresh water, most likely in a lacustrine environment. The fossiliferous material is dominated by woody debris, *Brachyphyllum* sp. and *Elatocladus* shoots. The only other *Elatocladus* identified in the region comes from a section of tephra and basalt near Potter Peak East where plant fossils are more abundant and include additional taxa such as *Equisetum laterale*, *Pagiophyllum feistmanteli* and *Cladophlebis antarctica* (Cantrill & Hunter, 2005; Hunter & Cantrill, 2006, this issue). It seems that these conifers preferred a volcanic-rich soil. Pillowed units, hyaloclastite, graded lapilli tuffs and rippled air-fall horizons within the volcanic facies confirm

https://doi.org/10.1017/S0016756806002597 Published online by Cambridge University Press

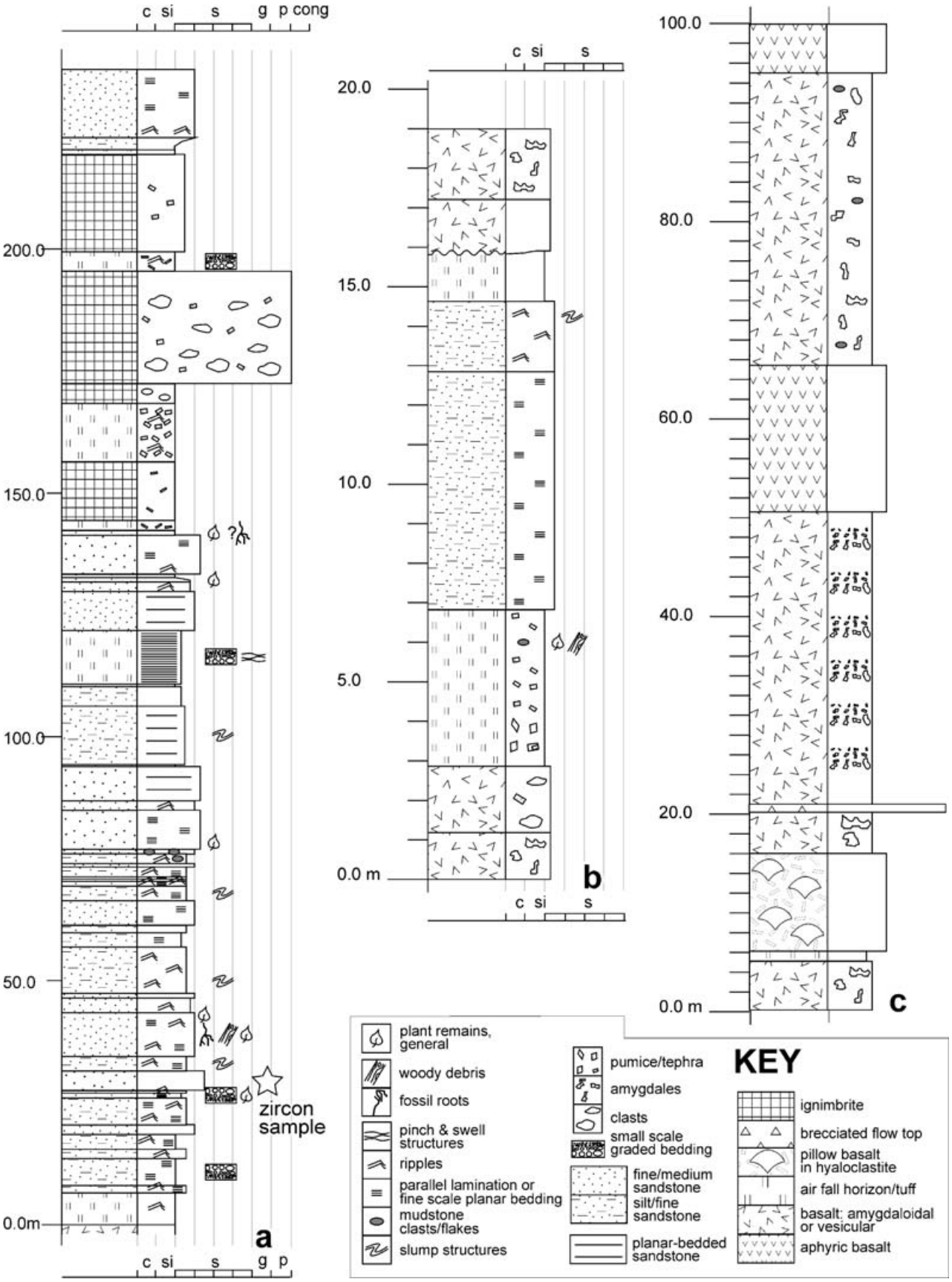

Figure 4. Logged sections through the Sweeney Formation. (a) Log of predominantly sedimentary section within the extracaldera facies from Potter Peak. (b) Log of sedimentary section at Mount Edward. (c) Log of basaltic facies from the southern exposure of the Sweeney Formation at Mount Jenkins.

https://doi.org/10.1017/S0016756806002597 Published online by Cambridge University Press

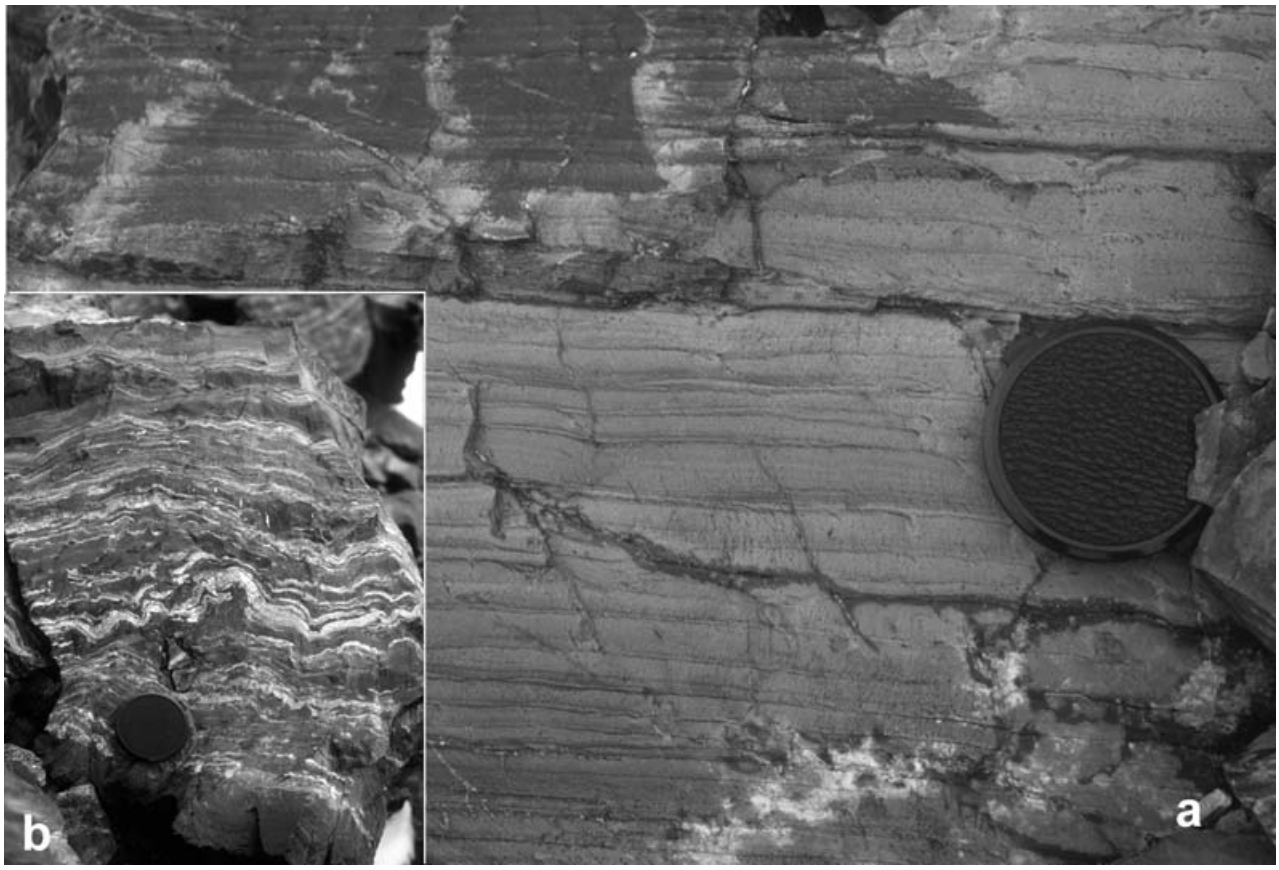

Figure 5. (a) Planar-bedded very fine sand/siltstone of the Sweeney Formation, Potter Peak West. (b) Disrupted and silicified bedding, Sweeney Formation, Mount Ballard. Lens cap is 52 mm diameter.

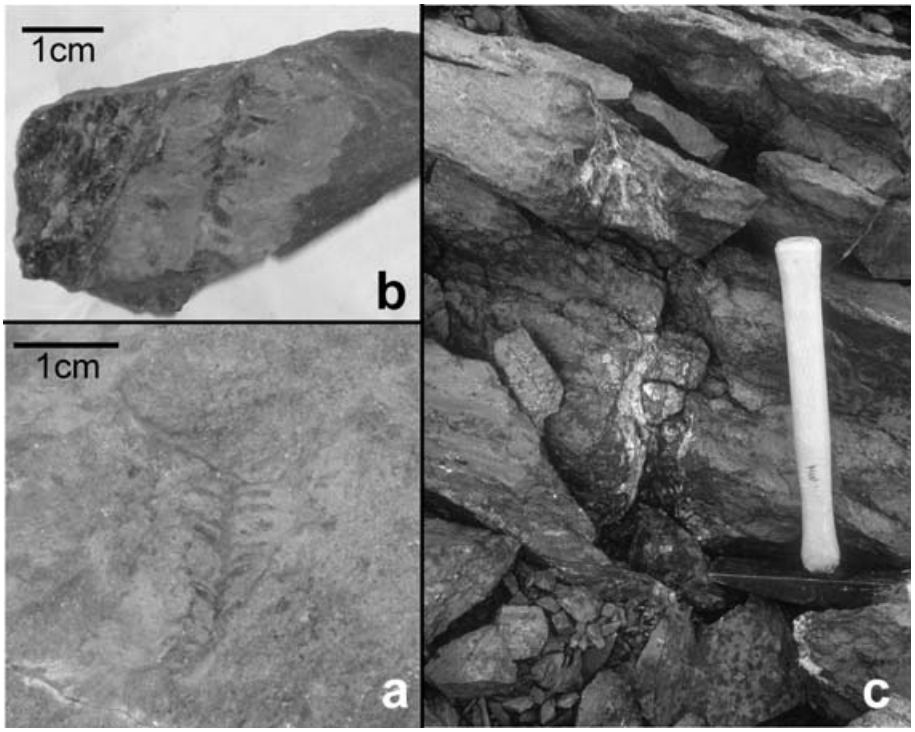

Figure 6. (a, b) Silicified wood, *Brachyphyllum* sp. and *Elatocladus confertus* shoots, Potter Peak West. (c) Cross-cutting roots up to 3 cm in diameter are consistent with the growth of conifers between eruptive phases. Length of hammer is 35 cm.

https://doi.org/10.1017/S0016756806002597 Published online by Cambridge University Press

eruption into or close to water. The volcanic and sedimentary units are interpreted as extracaldera facies. The contact with the Mount Poster Formation is always faulted or intruded and is interpreted as the caldera margin. The volcanic facies are dominated by basaltic lava flows and the sedimentary facies are consistent with wooded mountain slopes and lakes, established between eruptive phases.

Fossil content and age. Fossil plant material is the dominant element in the palaeoassemblage and points to a terrestrial environment. There is no evidence for marine organisms in the sequence. The material includes trunks and rooted horizons pointing to an *in situ* vegetation. Unfortunately, the material identified can only be placed in long-ranging Mesozoic groups suggestive of the Jurassic to Early Cretaceous. *Brachyphyllum* and *Elatocladus confertus* are long ranging and are recorded in the Botany Bay Group floras (e.g. Rees & Cleal, 2004) of Middle Jurassic age (Hunter *et al. 200*5) to the north, other Jurassic floras of the Latady Basin (e.g. Gee, 1989) and Early Cretaceous floras in the South Shetland Islands (Cantrill, 2000). As such they cannot be considered age diagnostic but suggestive of a Jurassic to Early Cretaceous (pre-Albian) age.

An absolute age for the Sweeney Formation is more difficult to determine, but a maximum age of 183 ± 4 Ma was obtained from the youngest detrital zircon peak measured on an extracaldera sandstone (see Section 3). This is consistent with contemporaneous deposition of the extracaldera facies and intracaldera volcanism.

3. Geochronology

3.a. Analytical method

U–Pb zircon analyses were performed by the NORDSIM Cameca 1270 ion-microprobe at the Swedish Natural History Museum, Stockholm. Zircons were separated, using standard heavy liquid and magnetic techniques, from several kilograms of crushed rock. Following hand-picking, the zircons were mounted in epoxy along with a few grains of the 1065 Ma Geostandards 91500 zircon standard (Wiedenbeck *et al.* 1995), and polished to expose the centres of the grains before optical and cathodoluminescence imaging. The mounts were cleaned and coated with 30 nm of gold prior to introduction into the ion-microprobe. Analytical procedure followed closely that of Whitehouse *et al.* (1997) and Whitehouse, Kamber & Moorbath (1999). Pb/U ratios were calibrated against the 91500 zircon standard using the measured UO_2/U ratios. The presence of common Pb was assessed by the measurement of ^{204}Pb. Analyses are uncorrected for common Pb except where statistically significantly high quantities were detected (the proportion of the ^{206}Pb that is common Pb exceeds ~ 1.75 %, Table 1) using the present-day terrestrial Pb value of Stacey & Kramers (1975). Errors for ratios and ages given in Table 1 are at the 1σ level and include the propagated errors of the standard measurements. Individual ages given in the text and figures are quoted at the 2σ level. Concordia average ages (Ludwig, 1998) and relative probability plots have been calculated using ISOPLOT version 3.1 (Ludwig, 1999) with the decay constants recommended by Steiger & Jäger (1977) and results are quoted throughout at the 2σ level.

3.b. Zircon petrography and U–Pb geochronology

Mount Poster Formation. Zircons were separated from eight samples of silicic ignimbrite cropping out within the Sweeney Mountains in the east to Lyon nunataks in the far west (Fig. 2). All of the eight ignimbrite samples share a common zircon morphology and cathodoluminescence (CL) character (Fig. 7). Zircons are dominated by bright, clear and colourless prisms, are typically 100–300 μm in length, have well-developed crystal facets, and have aspect ratios that range from 2:1 to 6:1. CL images reveal that for each sample some prisms are simple, with well-developed fine-scale growth zoning (e.g. Fig. 7b, grains 1 and 2) but more commonly grains exhibit weaker zoning (e.g. Fig. 7a, grain 1; 7g, grain 6; 7d, grain 9). All samples contain grains that are more complex and show core and rim structures. Typically, a CL-dark core is overgrown by a CL-bright rim. The rims are either homogeneous (e.g. Fig. 7a, grain 2; 7b, grain 3) or display weakly developed growth zoning (e.g. Fig. 7f, grain 16). The thickness of such overgrowths is also variable from a few microns (e.g. Fig. 7f, grain 17) to comprising the bulk of the grain (e.g. Fig. 7b, grain 2). U–Pb ion-microprobe geochronology (below) reveals that both simple prisms and zircon rims grew at the same time, most likely during volcanism. However, evidence that these magmas are highly contaminated is given not only by the zircon cores, but also by the fact that some of the simple prisms are inherited and have developed no zircon overgrowth during volcanism.

Seven of the eight samples yield indistinguishable concordia ages and demonstrate that simple prisms and zircon overgrowths developed between 185.2 ± 1.5 Ma and 181.1 ± 2.7 Ma (Fig. 8; Table 1). The weighted average of these ages is 183.4 ± 1.4 Ma. The remaining sample from Henry Nunataks (Fig. 2) yields a slightly younger age of 177.5 ± 2.2 Ma (Fig. 8; Table 1). Inherited grains yield Archaean, Palaeoproterozoic, Late Neoproterozoic–Cambrian, Carboniferous and Late Triassic–Early Jurassic ages (Table 1). These ages are in broad agreement with detrital zircon populations present in the Sweeney Formation sediment (below).

Sweeney Formation. Detrital zircons were separated from a well-sorted, fine-grained sandstone (R.8082.6) from the sedimentary facies at Potter Peak West (Figs 2, 3). The zircon crystals were moderately to well

https://doi.org/10.1017/S0016756806002597 Published online by Cambridge University Press

Table 1. U–Pb ion-microprobe data

Grain spot*	Anal†	f^{206}Pb (%)‡	^{207}Pb/^{206}Pb	± (%)	^{207}Pb/^{235}U	± (%)	^{206}Pb/^{238}U	± (%)	ρ	^{207}Pb/^{206}Pb age (Ma)	± Ma§	^{207}Pb/^{235}U age (Ma)	± Ma§	^{206}Pb/^{238}U age (Ma)	± Ma§	U (ppm)	Th (ppm)	Pb (ppm)	Th/U	Disc (%)¶
Mount Wasilewski (R.6871.3)																				
1	v*	1.26	0.0478	3.51	0.1884	3.84	0.0286	1.55	0.40	87	81	175	6	182	3	121	43	4	0.355	
2	r*	1.67	0.0522	5.33	0.2066	5.59	0.0287	1.69	0.30	293	117	191	10	183	3	97	45	3	0.467	
3	v*	0.54	0.0494	3.28	0.1920	3.62	0.0282	1.54	0.42	168	75	178	6	179	3	137	24	4	0.179	
4	v*	0.46	0.0526	3.24	0.2004	3.59	0.0276	1.54	0.43	311	72	185	6	176	3	218	55	7	0.253	
7	r	0.80	0.0549	4.22	0.2056	4.51	0.0272	1.59	0.35	408	92	190	8	173	3	86	36	3	0.419	
8	r	1.20	0.0555	3.58	0.2352	3.95	0.0307	1.68	0.42	433	78	214	8	195	3	119	39	4	0.330	−5.9
9	v*	1.74	0.0463	13.36	0.1860	13.44	0.0291	1.47	0.11	0	308	173	22	185	3	89	74	3	0.837	
11	r*	0.98	0.0493	2.73	0.1963	3.12	0.0289	1.51	0.48	163	63	182	5	183	3	184	40	6	0.216	
6	c	0.10	0.0504	1.39	0.2332	1.96	0.0336	1.39	0.71	212	32	213	4	213	3	642	67	23	0.105	
Lyon East (R.8125.1)																				
1	v*	0.67	0.0506	3.84	0.2021	4.19	0.0290	1.67	0.40	222	86	187	7	184	3	104	51	4	0.492	
2	v*	1.04	0.0489	3.42	0.1949	3.73	0.0289	1.49	0.40	142	78	181	6	184	3	131	57	5	0.436	
3	vc*	0.57	0.0479	3.41	0.1951	3.74	0.0295	1.52	0.41	97	79	181	6	187	3	129	40	4	0.311	
4	v*	1.07	0.0515	3.63	0.2040	3.96	0.0287	1.58	0.40	262	81	188	7	183	3	85	41	3	0.483	
5	v*	1.02	0.0511	2.98	0.1995	3.31	0.0283	1.43	0.43	247	67	185	6	180	3	142	83	5	0.585	
6	v*	1.03	0.0450	4.92	0.1830	5.14	0.0295	1.46	0.28	−58	116	171	8	188	3	194	184	8	0.948	
7	v*	1.15	0.0519	3.15	0.2103	3.47	0.0294	1.45	0.42	281	71	194	6	187	3	118	59	4	0.503	
8	c	0.07	0.0607	1.13	0.6977	2.06	0.0833	1.72	0.83	630	24	537	9	516	9	361	134	35	0.370	−8.0
10	c	0.03	0.1788	1.05	7.2733	1.74	0.2950	1.39	0.80	2642	17	2146	16	1666	20	356	230	144	0.645	−37.3
Henry Nunataks (R.8120.2)																				
1	v*	2.18	0.0507	4.28	0.1946	4.58	0.0278	1.64	0.36	228	96	181	8	177	3	71	30	2	0.425	
2	v*	0.38	0.0500	2.49	0.1920	2.88	0.0278	1.44	0.50	195	57	178	5	177	3	306	254	11	0.830	
4	v*	4.60	0.0500	2.88	0.1926	3.24	0.0279	1.48	0.46	197	66	179	5	178	3	185	178	7	0.962	
5	v*	0.29	0.0487	4.52	0.1900	4.80	0.0283	1.63	0.34	134	103	177	8	180	3	79	91	3	1.145	
6	v*	1.60	0.0500	3.56	0.1927	3.94	0.0280	1.70	0.43	195	81	179	6	178	3	136	49	4	0.357	
7	v*	1.22	0.0523	4.35	0.1996	4.63	0.0277	1.57	0.34	300	96	185	8	176	3	83	32	3	0.390	
3	i	1.37	0.0561	5.09	0.2313	5.28	0.0299	1.39	0.26	455	109	211	10	190	3	56	67	2	1.208	
Potter Peak West (R.7108.2)																				
1	v*	0.50	0.0495	4.14	0.1907	4.45	0.0279	1.61	0.36	173	94	177	7	178	3	214	56	7	0.262	
2	v*	0.39	0.0490	2.41	0.1948	2.81	0.0288	1.45	0.52	148	55	181	5	183	3	283	59	9	0.207	
3	r*	1.09	0.0542	3.57	0.2118	3.88	0.0283	1.52	0.39	381	78	195	7	180	3	113	44	4	0.392	
4	v*	0.74	0.0475	3.95	0.1882	4.25	0.0287	1.57	0.37	77	91	175	7	182	3	109	85	4	0.779	
7	v*	1.50	0.0509	3.75	0.2053	4.08	0.0293	1.60	0.39	237	84	190	7	186	3	116	80	4	0.692	
5	i	0.85	0.0500	2.44	0.2123	2.80	0.0308	1.38	0.49	196	56	195	5	195	3	323	82	11	0.253	
Lyon West (R.8122.5)																				
1	v*	0.58	0.0481	2.50	0.1944	2.87	0.0293	1.41	0.49	102	58	180	5	186	3	176	92	6	0.524	
4	v*	0.31	0.0489	2.89	0.1968	3.20	0.0292	1.36	0.43	145	66	182	5	185	2	138	188	6	1.360	
5	v*	0.62	0.0503	3.59	0.1970	3.83	0.0284	1.33	0.35	210	81	183	6	180	2	161	117	6	0.727	
6	v*	0.17	0.0505	2.00	0.1973	2.40	0.0284	1.34	0.56	217	46	183	4	180	2	285	124	10	0.433	
7	v*	1.10	0.0507	3.59	0.1994	3.83	0.0285	1.32	0.35	229	81	185	6	181	2	90	68	3	0.757	
8	v*	0.37	0.0514	3.55	0.2085	3.79	0.0294	1.32	0.35	259	80	192	7	187	2	92	51	3	0.554	
9	v*	0.78	0.0480	2.90	0.1938	3.19	0.0293	1.33	0.42	98	67	180	5	186	2	132	89	5	0.675	
2	c	0.02	0.1044	0.34	3.8957	1.37	0.2706	1.33	0.97	1704	6	1613	11	1544	18	966	102	298	0.106	−7.7
3	i	2.02	0.0601	5.67	0.8015	5.82	0.0967	1.32	0.23	607	118	598	27	595	8	55	20	6	0.366	
Mount Jenkins (R.7103.1)																				
9	v*	0.37	0.0509	2.44	0.2043	2.65	0.0291	1.02	0.39	234	55	189	5	185	2	222	50	7	0.226	
10	v*	1.39	0.0514	4.25	0.2063	4.40	0.0291	1.14	0.26	257	95	190	8	185	2	72	41	3	0.569	
11	v*	0.57	0.0494	2.88	0.1979	3.07	0.0291	1.04	0.34	167	66	183	5	185	2	164	40	5	0.242	
14	v*	1.52	0.0489	4.28	0.1987	4.40	0.0295	1.04	0.24	141	97	184	7	187	2	74	42	3	0.567	
15	v*	0.52	0.0496	3.96	0.1983	4.11	0.0290	1.10	0.27	177	90	184	7	184	2	106	51	4	0.484	
16	v*	0.25	0.0496	3.76	0.1970	3.91	0.0288	1.06	0.27	179	85	183	7	183	2	89	43	3	0.482	
18	v*	0.40	0.0508	3.14	0.2068	3.36	0.0295	1.18	0.35	233	71	191	6	187	2	146	90	5	0.618	

12	i	0.61	0.0503	3.02	0.2091	3.20	0.0301	1.05	0.33	209	69	193	6	191	2	154	122	6	0.790	
13	i	0.56	0.0515	3.56	0.2123	3.71	0.0299	1.06	0.28	261	80	195	7	190	2	103	62	4	0.604	
17	c	0.44	0.0496	3.76	0.1970	3.91	0.0288	1.06	0.27	224	72	197	6	194	2	132	152	6	1.149	
2	c	0.03	0.0583	1.71	0.7441	1.92	0.0926	0.89	0.46	539	37	565	8	571	5	143	135	18	0.941	
3	i	0.14	0.0578	1.57	0.6957	1.79	0.0873	0.87	0.49	522	34	536	7	540	5	130	108	15	0.829	
19	i	0.02	0.1881	0.36	13.4219	1.12	0.5175	1.07	0.95	2726	6	2710	11	2689	23	225	131	157	0.581	
Sky Hi Nunataks (R.6878.1)																				
1	v*	0.98	0.0543	3.62	0.2157	3.77	0.0288	1.07	0.28	385	79	198	7	183	2	97	38	3	0.388	
2	v*	1.48	0.0489	4.03	0.1983	4.18	0.0294	1.12	0.27	145	92	184	7	187	2	86	44	3	0.510	
4	v*	0.91	0.0530	4.01	0.2056	4.16	0.0282	1.08	0.26	327	89	190	7	179	2	80	60	3	0.757	
7	v*	0.09	0.0495	1.54	0.2023	2.07	0.0296	1.39	0.67	173	36	187	4	188	3	877	44	28	0.050	
8	v*	0.67	0.0513	3.88	0.2049	4.14	0.0290	1.47	0.35	253	87	189	7	184	3	130	30	4	0.232	
9	v*	0.64	0.0490	4.74	0.1935	4.95	0.0286	1.44	0.29	150	107	180	8	182	3	113	71	4	0.629	
10	v*	0.49	0.0502	3.16	0.1993	3.48	0.0288	1.45	0.42	206	72	185	6	183	3	220	44	7	0.200	
11	v*	1.47	0.0513	4.40	0.2000	4.66	0.0282	1.52	0.33	256	98	185	8	180	3	120	85	4	0.707	
12	v*	1.09	0.0505	5.11	0.1985	5.34	0.0285	1.54	0.29	218	114	184	9	181	3	88	37	3	0.420	
3	i	0.71	0.0481	4.34	0.1975	4.46	0.0298	1.04	0.23	104	100	183	8	189	2	206	28	7	0.136	
5	c	0.41	0.0490	2.97	0.2069	3.14	0.0306	1.03	0.33	147	68	191	5	194	2	345	174	13	0.503	
6	i	0.31	0.0496	1.87	0.2123	2.13	0.0311	1.03	0.48	175	43	196	4	197	2	394	147	14	0.373	
Mount Ballard (R.6888.2)																				
1	v*	1.38	0.0508	5.09	0.1974	5.29	0.0282	1.44	0.27	234	113	183	9	179	3	84	46	3	0.551	
3	v*	0.59	0.0491	3.14	0.1948	3.49	0.0288	1.52	0.43	152	72	181	6	183	3	230	155	8	0.673	
4	v*	0.70	0.0482	4.69	0.1896	4.92	0.0285	1.48	0.30	109	107	176	8	181	3	140	47	5	0.338	
5	v*	0.95	0.0479	5.65	0.1884	5.89	0.0285	1.69	0.29	93	129	175	10	181	3	115	72	4	0.623	
2	i	0.89	0.0504	5.27	0.3539	5.54	0.0509	1.74	0.31	215	118	308	15	320	5	117	104	9	0.886	
Sweeney Formation (R.8082.6)																				
1	d	0.11	0.0736	1.01	1.6408	1.82	0.1617	1.51	0.83	1030	20	986	12	966	14	347	220	71	0.635	
2	d	1.96	0.0514	3.69	0.2016	3.95	0.0285	1.41	0.36	258	83	186	7	181	3	154	66	5	0.428	
3	d	1.03	0.0575	2.39	0.6236	2.76	0.0787	1.38	0.50	509	52	492	11	488	6	113	60	11	0.532	
4	d	0.90	0.0576	1.25	0.4839	1.90	0.0609	1.43	0.75	514	27	401	6	381	5	517	274	39	0.530	−12.6
5	d	0.21	0.0772	1.70	1.8695	2.20	0.1757	1.40	0.64	1125	33	1070	15	1044	14	148	105	34	0.711	
6	d	0.83	0.0618	0.83	0.7356	1.61	0.0863	1.38	0.86	667	18	560	7	534	7	710	401	76	0.564	−13.1
7	d	7.80	0.0530	9.71	0.6238	9.81	0.0853	1.39	0.14	331	207	492	39	528	7	153	74	15	0.483	
8	d	0.09	0.0578	1.19	0.6396	1.83	0.0803	1.39	0.76	521	26	502	7	498	7	405	263	43	0.648	
9	d	0.31	0.0561	1.83	0.6686	2.29	0.0864	1.38	0.60	456	40	520	9	534	7	149	46	15	0.306	
10	d	0.10	0.0772	1.78	1.9481	2.35	0.1830	1.54	0.65	1127	35	1098	16	1083	15	114	46	25	0.401	
11	d	0.65	0.0648	1.48	1.0425	2.22	0.1167	1.65	0.74	768	31	725	12	711	11	160	156	26	0.974	
12	d	0.57	0.0722	2.40	1.4937	2.77	0.1500	1.38	0.50	992	48	928	17	901	12	97	58	19	0.593	
13	d	0.03	0.0682	0.71	1.2900	1.55	0.1371	1.38	0.89	875	15	841	9	828	11	590	134	91	0.228	
14	d	0.24	0.0583	1.85	0.6824	2.31	0.0849	1.39	0.60	541	40	528	10	525	7	160	37	15	0.229	
15	d	0.14	0.2224	0.66	18.1206	1.63	0.5911	1.49	0.91	2998	11	2996	16	2994	36	86	85	75	0.992	
16	d	6.04	0.0543	9.21	0.4928	9.32	0.0658	1.43	0.15	383	195	407	32	411	6	192	144	16	0.749	
17	d	0.09	0.2651	0.64	21.2336	1.62	0.5810	1.49	0.92	3277	10	3149	16	2953	35	173	31	131	0.181	−8.8
18	d	0.23	0.0737	1.37	1.7085	1.94	0.1681	1.38	0.71	1034	27	1012	13	1001	13	125	127	29	1.014	
19	d	5.99	0.0678	5.45	0.9109	5.63	0.0975	1.42	0.25	862	109	658	28	600	8	157	97	19	0.618	
20	d	0.22	0.0495	1.53	0.1986	2.07	0.0291	1.39	0.67	170	35	184	3	185	3	896	609	33	0.680	
21	d	0.33	0.0522	1.43	0.2640	2.01	0.0367	1.41	0.70	295	32	238	4	232	3	675	446	31	0.662	
22	d	0.34	0.0599	1.31	0.7448	1.90	0.0902	1.38	0.73	600	28	565	8	557	7	301	259	35	0.859	
23	d	1.75	0.0646	1.52	1.0458	2.06	0.1174	1.39	0.67	761	32	727	11	716	9	1019	64	129	0.063	
24	d	0.07	0.0726	0.63	1.5381	1.52	0.1536	1.38	0.91	1004	13	946	9	921	12	668	225	121	0.337	−4.1

Uncertainties given at the 1σ level.
*Spot identification number.
†Portion of zircon analysed as interpreted from CL images: v – volcanic, r – rim, c – core, i – inherited (without rim), d – detrital; *indicates included in age calculation.
‡Fraction of ^{206}Pb that is common Pb (calculated from ^{204}Pb).
§Age errors have included the propagated errors of the standard measurements.
[1]Age discordance from 2σ limits in conventional concordia space.

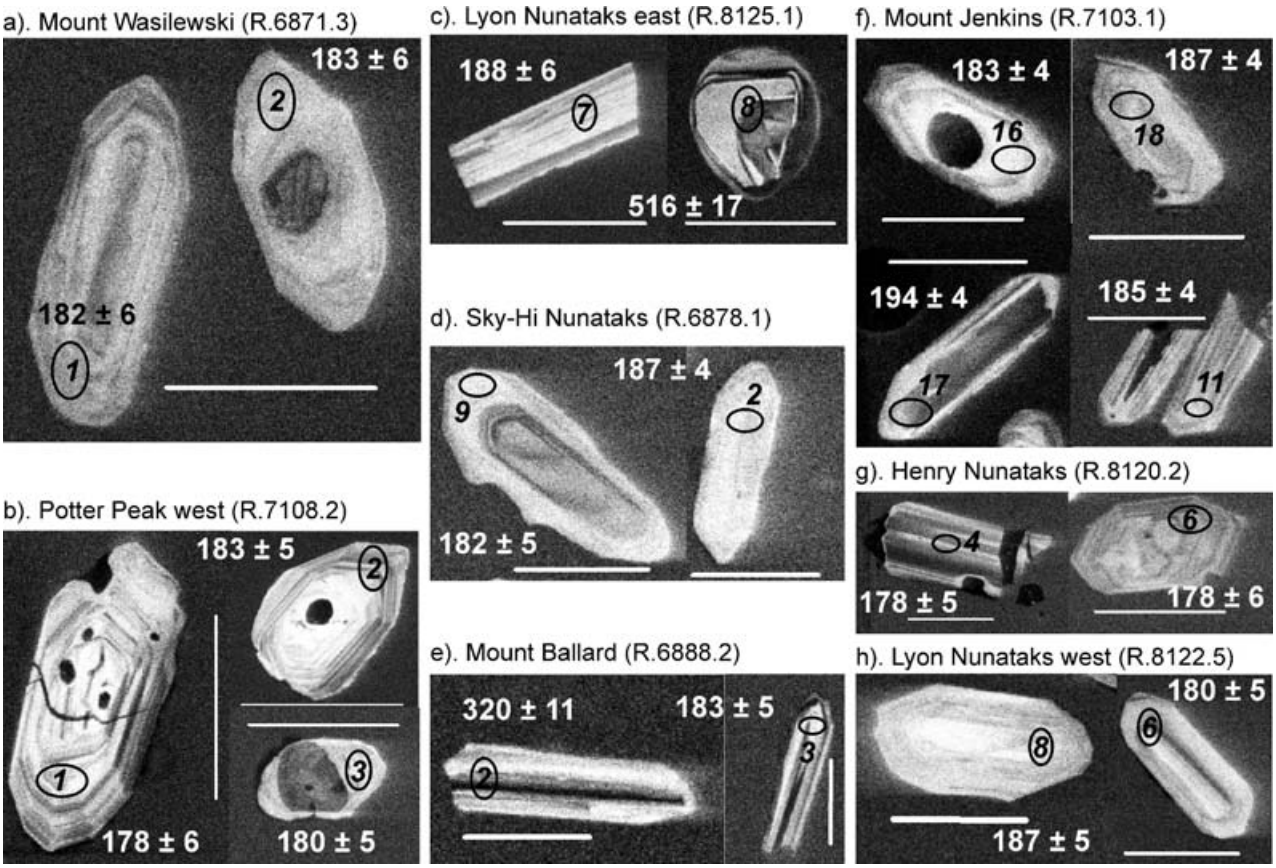

Figure 7. CL images of representative zircons for each of the Mount Poster Formation volcanic samples selected for geochronology. Ellipses indicate the location of the ion-microprobe spot and the number within or adjacent to the ellipse corresponds to the sample identification number given in Table 1. Ages given in white are $^{206}Pb/^{238}U$ ages and are given with 2σ errors. Scale bar on all figures is 150 μm.

rounded, mostly clear and colourless, typically 100–150 μm in diameter and ovoid, with only a few elongate needles present. Under CL, grains were variably fluorescent and often exhibited a complex internal structure; such a pattern is expected for detrital zircons with a varied source. Where zircon overgrowths were large enough, these were analysed in preference to the core. However, zircon overgrowths were found to vary in age. Although the dataset is small, detrital zircon populations in the Archaean, Late Mesoproterozoic–Cambrian, Devonian, Triassic and Early Jurassic are present (Fig. 9). The two youngest grains yield a concordia age of 183 ± 4 Ma and demonstrate that the sedimentary rocks were deposited during or after Early Jurassic times.

3.c. Interpretation

Mount Poster Formation. We interpret the concordia ages (Fig. 8) as dating zircon growth associated with volcanism in eastern Ellsworth Land and zircon growth probably occurred either within an evolving magma chamber or during eruption. Inherited grains that did not develop overgrowths were probably incorporated from wall rocks or the substrate during the eruption.

A *c.* 183 Ma age for the majority of ignimbrites is slightly younger than the *c.* 188 Ma ages obtained by Fanning & Laudon (1999) but compares favourably with the age of Karoo-Ferrar volcanism (183 Ma: Riley & Knight, 2001). Intriguingly, inherited grains with ages between 195 and 185 Ma are present in five of the eight analysed samples and suggest that a phase of volcanism may have occurred prior to the more voluminous products of *c.* 183 Ma volcanism. Moreover, volcanism continued after the main phase of *c.* 183 Ma volcanism, as is recorded at Henry Nunataks (177.5 ± 2.2 Ma).

Sweeney Formation. The age distribution of detrital zircons from the Sweeney Formation compares well with those obtained from the Latady Formation and other older sedimentary sequences within West Antarctica (British Antarctic Survey, unpub. data; Millar *et al.* 2003; Laudon & Fanning, 2003; Flowerdew *et al.* 2004). Excluding the youngest Jurassic zircons, these were likely to have been sourced from zircons either recycled from sedimentary sequences believed

https://doi.org/10.1017/S0016756806002597 Published online by Cambridge University Press

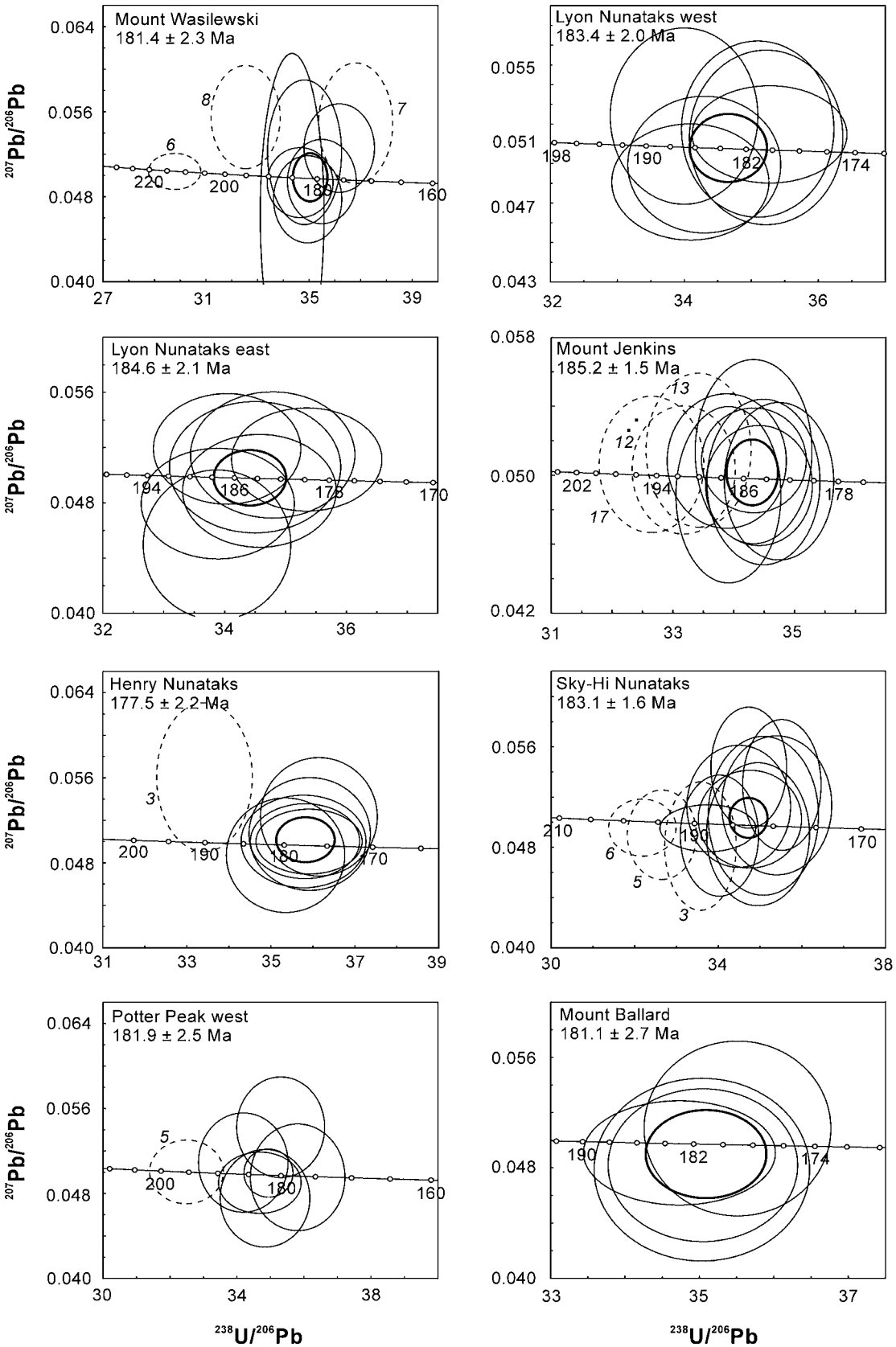

Figure 8. Tera-Wasserburg concordia diagrams for Mount Poster Formation volcanics. Locality and calculated age are shown in the top left of each concordia diagram. Ellipses are plotted with 2σ errors and concordia ages are quoted at the 2σ level. Ellipses not included in the age calculations are dashed and have an adjacent spot identification corresponding to the analysis in Table 1. Analyses omitted in age calculations are interpreted to be inherited or to have suffered from Pb-loss.

https://doi.org/10.1017/S0016756806002597 Published online by Cambridge University Press

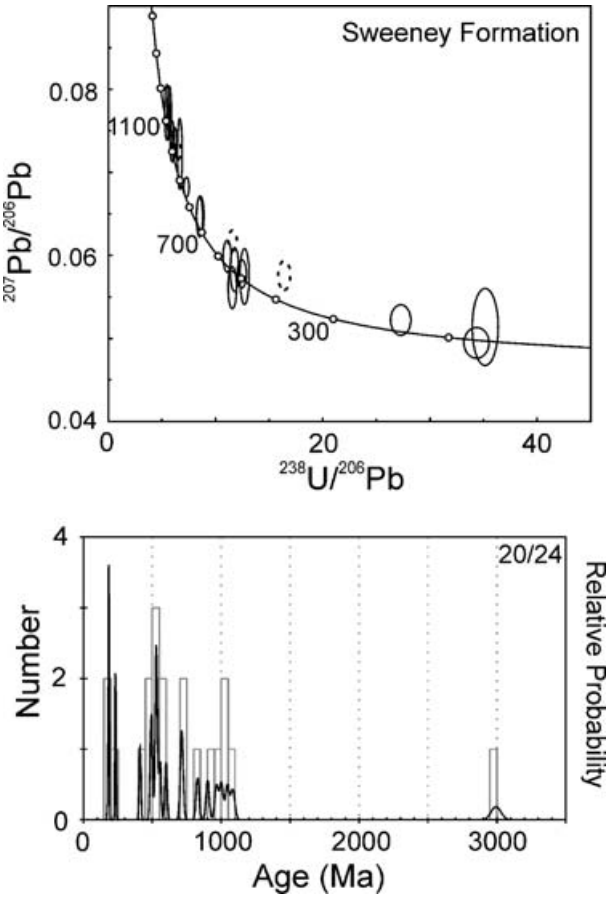

Figure 9. Tera-Wasserburg concordia diagram and relative probability plot for Sweeney Formation sediment. For the concordia diagram, ellipses are plotted at the 2σ level and analyses with a 5 % or greater error on the $^{207}Pb/^{206}Pb$ ratio are omitted. Analyses that are discordant on the 2σ ellipse are dashed. For the relative probability plot only concordant data (where the 2σ error ellipse intersects concordia) are considered.

to underlie the Mount Poster Formation, such as the Permian Erewhon Beds (Laudon, 1991) or the magmatic products within the Antarctic Peninsula that were generated through a periodically active Gondwana margin throughout the Palaeozoic and Mesozoic (Millar *et al.* 2001; Millar, Pankhurst & Fanning, 2002). The youngest detrital zircons are the same age as the Mount Poster Formation, allowing deposition of the Mount Poster and Sweeney formations to be broadly contemporaneous. Such a conclusion is in keeping with the field evidence that demonstrates the deposition of the Sweeney Formation occurred between episodes of volcanism and is consistent with coeval deposition of the extracaldera and intracaldera formations. Given the contemporaneous Mount Poster and Sweeney formations, it is surprising that the Sweeney Formation is not characterized by volcanic-derived detritus, as is seen at Botany Bay in the northeast Antarctic Peninsula (Hunter *et al.* 2005). At Botany Bay, deposition is contemporaneous with major silicic volcanism at *c.* 167 Ma. The lack of Jurassic-age zircons present in the Sweeney Formation is not easily explained, but may be due to a sampling bias. Alternatively, and more likely, is that either (1) the associated basaltic volcanism is zircon-poor and so will not contribute many Jurassic zircons; (2) local drainage patterns did permit a Mount Poster Formation source but perhaps reworked pre-Jurassic sedimentary sequences; (3) there is a tectonic reason, that is, it was deposited elsewhere, but moved to its current position by strike-slip faulting; or (4) that the Sweeney Formation was deposited prior to the main phase of silicic volcanism.

4. Petrology, geochemistry and petrogenesis

Analytical techniques. Rb–Sr whole rock analyses were carried out at the NERC Isotope Geosciences laboratory, Keyworth. Sr isotope compositions were determined on a Finnegan-MAT 262 mass-spectrometer using static multicollection, to an internal precision of better than 10 ppm (1 sem) and Nd isotope compositions were run on the Triton. The $^{87}Sr/^{86}Sr$ ratios were further normalized to a nominal value of 0.710249 ± 3 (1σ) for the NBS987 standard. Nine analyses of the in-house J&M Nd isotope standard gave a value of 0.511191 ± 16 (1σ); reported $^{143}Nd/^{144}Nd$ values were normalized to a value of 0.511123 for this standard.

Major and selected trace element analysis was by standard XRF techniques at the Department of Geology, University of Keele, with methods detailed by Floyd (1986). Higher-precision trace element abundances were determined by inductively coupled plasma mass spectrometry (ICP-MS) at the University of Durham. The analytical methods, precision and detection limits are comparable with those detailed by Pearce *et al.* (1995).

4.a. Mount Poster Formation

Petrographically, the rhyolites contain abundant phenocrysts of plagioclase, sanidine, hornblende, embayed quartz and Fe–Ti oxides, with an alteration assemblage of sericite, clay minerals and calcite (Riley *et al.* 2001). The rhyolitic ignimbrites have undergone lower greenschist facies metamorphism and have an apparent porphyritic texture, comprising abundant feldspar crystals that occur as single euhedra or clusters.

Riley *et al.* (2001) investigated the geochemistry and petrogenesis of the Mount Poster Formation, which is summarized here alongside data reported from this study (Table 2). The silicic volcanic rocks plot on the boundary between dacite and rhyolite on a total alkali–silica plot (Fig. 10). Riley *et al.* (2001) further subdivided the rhyolites into a high-Ti (> 0.7 wt % TiO_2), at 70–74 wt % SiO_2, and a low-Ti group (< 0.4 wt % TiO_2), at > 76 wt % SiO_2, which corresponded to their geological setting. The

https://doi.org/10.1017/S0016756806002597 Published online by Cambridge University Press

Table 2. Whole rock analyses of basalt lavas from the Sweeney Formation

Sample	R.8087.1	R.8090.6	R.8091.3	R.8095.3	R.8109.2	R.8082.1	R.6890.5*	R.6900.2*	R.7106.2*	R.7114.3*	R.8120.2	R.8122.5	R.8125.1	R.6878.1
Latitude (S)	75°08.99′S	75°06.50′S	75°11.61′S	75°12.94′S	75°12.58′S	75°08.52′S	75°12.95′S	75°11.59′S	75°08.99′S	74°06.58′S	75°07.89′S	74°49.97′S	74°49.14′S	74°53.41′S
Longitude	068°49.11′W	069°16.29′W	069°15.31′W	069°38.06′W	070°47.77′W	068°47.63′W	070°03.43′W	069°15.28′W	068°49.05′W	069°15.60′W	072°34.34′W	073°55.41′W	073°46.47′W	071°15.58′W
	AB	OT	AB	QT	QT	AB	AB	QT	AB	OT				
SiO_2	46.24	45.98	45.91	48.68	46.63	50.34	46.87	50.27	47.63	46.26	68.13	68.70	68.16	70.41
TiO_2	1.50	1.71	0.68	1.27	1.67	1.23	0.90	0.59	1.36	0.55	0.88	0.81	0.92	0.75
Al_2O_3	16.57	13.42	15.74	16.02	14.88	13.09	15.73	15.65	13.89	16.59	14.01	13.60	13.72	12.94
Fe_2O_3(T)	10.32	14.26	11.71	11.49	14.52	12.32	12.87	9.05	10.41	10.22	5.67	5.37	5.73	5.06
MnO	0.15	0.22	0.32	0.20	0.22	0.21	0.21	0.17	0.16	0.17	0.07	0.06	0.05	0.09
MgO	8.54	9.10	10.19	8.81	7.89	7.32	10.14	8.32	10.36	10.65	1.38	1.16	1.13	1.67
CaO	9.13	10.28	8.78	8.75	10.29	6.01	5.44	10.75	8.86	10.93	2.48	2.38	1.64	1.42
Na_2O	2.90	1.82	2.97	2.15	1.74	3.47	3.16	2.16	2.80	1.39	2.12	2.15	2.30	2.05
K_2O	0.74	0.09	0.12	0.10	0.40	1.31	0.39	0.63	0.83	0.06	4.02	4.08	3.84	5.00
P_2O_5	0.18	0.17	0.05	0.13	0.17	0.11	0.09	0.05	0.20	0.05	0.24	0.19	0.25	0.20
LOI	3.36	2.50	3.12	2.18	1.32	4.49	4.68	1.82	3.10	3.16	1.45	1.27	2.15	0.77
Total	**99.63**	**99.55**	**99.60**	**99.77**	**99.75**	**99.90**	**100.48**	**99.44**	**99.58**	**100.04**	**100.44**	**99.78**	**99.90**	**100.35**
Sc	34.6	37.8	42.8	40.2	42.4	33.9					13.1	14.3	15.7	
Cr	382.1	391.45	159.65	292.59	175.46	235.16	606	142	635	119	28.5	21.6	30.8	28.0
Ni	198	194	211	157	114	140	242	167	289	231	15	11	15	16
Co	47.8	55.4	56.1	52.1	56.1	48.0					11.0	10.3	12.2	
Ga	15.71	17.84	13.78	16.16	18.89	16.69	17	10	17	14	18.01	17.77	18.77	
Rb	12.10	0.48	2.07	3.84	11.95	20.93	15	20	24	9	188.50	190.37	203.74	200.24
Sr	513.1	118.3	166.4	119.3	126.0	91.7	65	293	404	132	154.4	165.9	166.6	129.7
Y	25.4	33.7	16.5	25.4	36.2	27.6	21	16	23	16	48.6	46.0	50.7	47.9
Zr	94.8	75.0	17.4	58.3	73.0	75.1	44	58	116	34	114	101	73	327
Nb	10.72	6.86	1.39	4.66	7.91	3.59	5	5	14		18.29	17.01	19.63	16.48
Cs	2.64	0.44	0.44	1.18	2.35	1.33					6.15	4.60	8.38	8.30
Ba	285	31	12	60	122	501	135	241	448		801	801	817	875
La	7.8	7.4	2.0	4.1	7.5	5.0					48.3	47.8	54.5	45.6
Ce	18.1	17.6	4.4	10.3	17.6	12.5					97.5	94.8	107.5	97.6
Pr	2.78	2.74	0.79	1.69	2.70	1.96					12.59	11.90	14.07	12.00
Nd	13.5	13.6	4.2	9.0	13.5	9.6					50.6	46.8	56.0	48.9
Sm	3.80	4.17	1.50	2.94	4.13	2.99					10.17	9.32	10.98	9.60
Eu	1.39	1.41	0.60	0.94	1.39	0.92					1.68	1.57	1.85	1.58
Gd	4.67	5.26	2.21	4.00	5.41	3.95					9.46	8.83	10.19	9.10
Tb	0.77	0.92	0.41	0.70	0.97	0.71					1.45	1.34	1.54	1.36
Dy	4.61	5.84	2.70	4.37	6.02	4.63					8.31	7.80	8.82	7.87
Ho	0.94	1.20	0.58	0.93	1.29	0.99					1.63	1.55	1.72	1.65
Er	2.52	3.23	1.61	2.56	3.51	2.73					4.32	4.16	4.56	4.51
Tm	0.37	0.50	0.25	0.39	0.54	0.43					0.67	0.65	0.71	0.68
Yb	2.34	3.10	1.59	2.42	3.34	2.82					4.04	3.95	4.21	4.50
Lu	0.38	0.47	0.25	0.39	0.51	0.45					0.64	0.63	0.65	0.70
Hf	2.64	2.37	0.72	1.63	2.15	2.20					3.38	3.19	2.44	8.00
Ta	0.71	0.45	0.11	0.31	0.51	0.25					1.27	1.28	1.35	1.36
Pb	0.66	1.31	1.33	1.14	1.68	4.58					26.31	28.92	26.56	25.10
Th	1.15	1.20	0.21	0.46	1.20	1.46					17.73	17.31	18.98	18.60
U	0.40	0.25	0.06	0.09	0.27	0.40					3.13	3.78	3.26	3.58
Rb	12.10	0.48	2.07	3.84	11.95						188.50	190.37	203.74	200.24
Sr	513.1	118.3	166.4	119.3	126.0						154.4	165.9	166.6	129.7
$^{87}Rb/^{86}Sr$	0.06041	0.02431	0.03444	0.09257	0.29151						3.48737	3.44916	3.19613	4.46564
$^{87}Sr/^{86}Sr_n$	0.710273	0.705588	0.707259	0.706052	0.705656						0.729343	0.727152	0.727356	0.730694
$^{87}Sr/^{86}Sr_{183}$	0.710118	0.705526	0.707171	0.705815	0.704910						0.720418	0.718325	0.719176	0.719265
Sm	3.67	3.94	1.46	2.87	4.07						10.19	9.17	10.60	9.54
Nd	12.75	12.71	4.03	8.60	13.00						49.43	45.07	52.46	47.01
$^{147}Sm/^{144}Nd$	0.1742	0.1876	0.2190	0.2020	0.1893						0.1246	0.1230	0.1222	0.1227
$^{143}Nd/^{144}Nd_n$	0.512848	0.512809	0.512872	0.512918	0.512802						0.512103	0.512140	0.512112	0.512126
εNd_{183}	4.6	3.5	4.1	5.3	3.4						−8.8	−8.0	−8.6	−8.3

*XRF only; AB – alkali basalt; OT – olivine tholeiite; QT – quartz tholeiite.

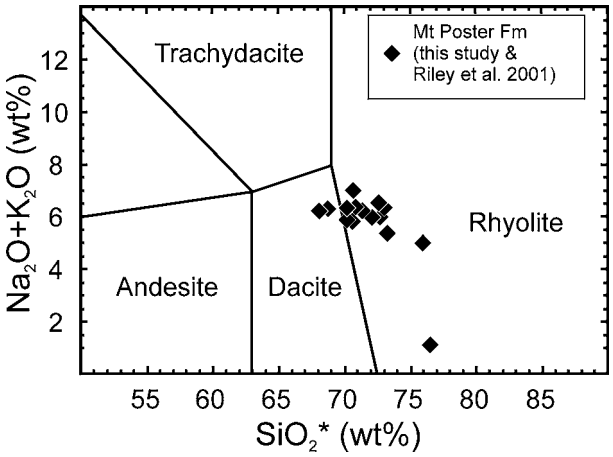

Figure 10. Total alkali v. SiO_2 plot for the Early Jurassic silicic rocks of the Mount Poster Formation (this study and Riley *et al.* 2001). SiO_2 is recalculated to volatile-free totals of 100 % (SiO_2*).

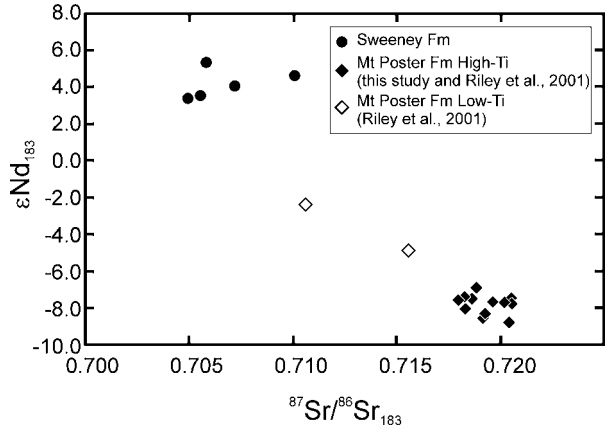

Figure 11. εNd_{183} v. $^{87}Sr/^{86}Sr_{183}$ plots for volcanic rocks from the Sweeney and Mount Poster formations. The diamond symbols are from Riley *et al.* (2001) and the circle symbols are from this study.

high-Ti group occurs within the intracaldera rocks, while the low-Ti group corresponds to the extracaldera succession. The newly defined Mount Poster Formation rhyolites all fall into the high-Ti, intracaldera group. The low-Ti rhyolites are all extracaldera volcanic rocks, which typically occur as thinner, strongly welded ignimbrite sheets, in contrast to the thick units of the main caldera rhyolites.

A total of 12 rhyolite samples (four in this study; eight in Riley *et al.* 2001) from the Mount Poster Formation have been analysed for Sr and Nd isotope ratios (Table 2). Ratios have been corrected to initial values using an eruption age of 183 Ma (see Section 3). The $^{87}Sr/^{86}Sr$ ratios are considerably more radiogenic than the rhyolites of the Middle Jurassic Mapple Formation or the extracaldera low-Ti group (Riley *et al.* 2001), and they form a relatively tight cluster in both $^{87}Sr/^{86}Sri$ (0.7180–0.7206) and εNdi (-6.9 to -8.8) (Fig. 11).

Riley *et al.* (2001) concluded that the small isotopic range exhibited for such a large volume of rhyolite suggested residence in a long-lived, convecting magma chamber in order to achieve homogenization. The caldera-related setting indicated that the magma chamber was situated in the upper crust, while the strongly radiogenic $^{87}Sr/^{86}Sr$ ratios and negative εNd values are consistent with a significant component of middle–upper crust in their petrogenesis.

4.b. Sweeney Formation basaltic facies

Extracaldera basalts of the Sweeney Formation are rare but their petrogenesis is important within the context of generation of large volumes of silicic magmatism at this time. The basalts selected vary from aphyric, to feldspar phyric, to amygdaloidal basalts. They are generally altered and contain abundant feldspar and clinopyroxene, with additional sparse phases of apatite, titanomagnetite and orthopyroxene. The plagioclase and clinopyroxene phenocrysts are typically euhedral, although the clinopyroxene is extensively altered. No olivine was identified in the groundmass or as a phenocryst phase.

The ten basalts selected include olivine and quartz tholeiites, as well as transitional to alkali basalts (Table 2). They are characterized by moderate- to high-Mg numbers (52–66) and SiO_2 values of 45.9–50.3 wt %. Compositionally, they are all basaltic (Fig. 12). Three of the samples (R.6900.2, R.7106.1, R.7114.3) can be considered primitive with $FeO^*/MgO < 1$, and Ni contents up to 289 ppm and Cr up to 635 ppm. The remaining samples also have high Cr and Ni contents, but have undergone at least some fractional crystallization.

Six of the samples have been analysed for rare earth element (REE) contents. The samples all have minor negative Eu anomalies indicating small amounts

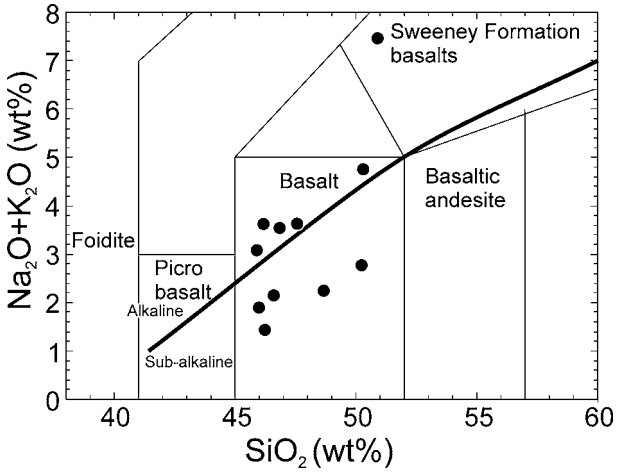

Figure 12. Total alkali v. SiO_2 plot for the Early Jurassic basaltic rocks of the Sweeney Formation. All rocks are basaltic in composition, but include alkali basalts as well as tholeiites.

https://doi.org/10.1017/S0016756806002597 Published online by Cambridge University Press

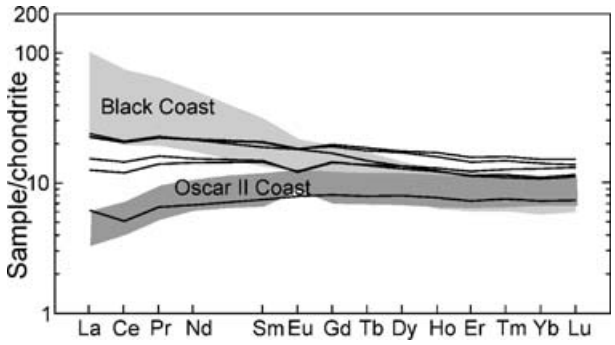

Figure 13. Chondrite normalized (Nakamura, 1974) rare earth element abundances in Sweeney Formation basalts. The data are compared to mafic dykes from the Oscar II Coast and the Black Coast (Leat *et al*. 2002).

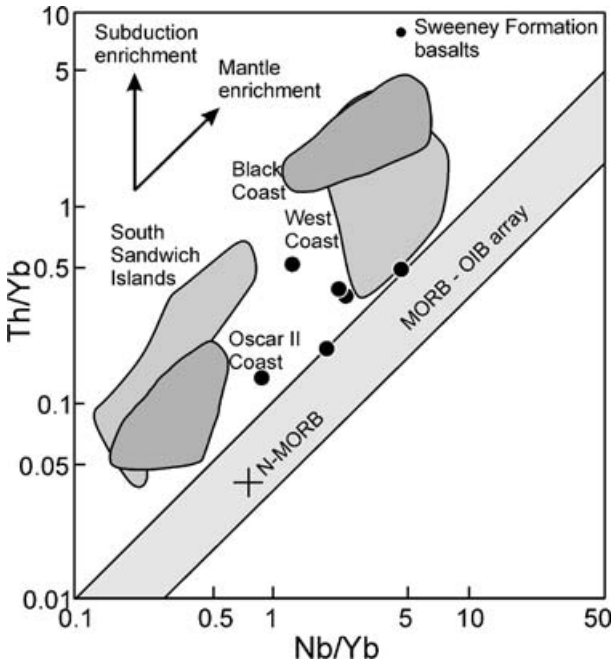

Figure 14. Th/Yb v. Nb/Yb plot showing the composition of basaltic rocks from the Sweeney Formation relative to the MORB-OIB array of Pearce & Peate (1995). The fields of the mafic dykes from the Oscar II and Black coasts (Leat *et al.* 2002) are shown, along with those of the South Sandwich Islands (Pearce *et al.* 1995) and the Antarctic Peninsula west coast (Scarrow *et al.* 1998).

of plagioclase fractionation, and flat REE patterns with (La/Yb)N ~ 1. The Sweeney Formation basalts are plotted in comparison to mid-Cretaceous basaltic dykes (Leat *et al.* 2002) of the Antarctic Peninsula (Fig. 13) and (with the exception of one sample) are intermediate between the asthenosphere-derived dykes of the Oscar II Coast (northeast Antarctic Peninsula) and the lithosphere-derived dykes of the Black Coast (southeast Antarctic Peninsula). The Nb/Yb v. Th/Yb diagram (Fig. 14) reinforces the conclusion of the REE diagram that the Sweeney Formation basalts are typically intermediate between asthenosphere- and lithosphere-derived sources. Several of the samples plot close to the mantle array, indicating that they have little or no subduction-modified component. Isotopically the basalts also have an asthenosphere-dominated signature with $^{87}Sr/^{86}Sr$ (0.7049–0.7072) and εNd (3.4–5.3) with one slightly more radiogenic sample having $^{87}Sr/^{86}Sr$ of 0.7101 (Fig. 11).

The widespread Jurassic-age silicic volcanism of Patagonia and the Antarctic Peninsula is characterized by only minor amounts of associated mafic volcanism. The Sweeney Formation basalts have significantly different $^{87}Sr/^{86}Sr$ and εNd values from the presumably coeval rhyolites of the Mount Poster Formation, indicating there is no simple relationship between them involving fractional crystallization. The petrogenetic model for rhyolite generation proposed by Riley *et al.* (2001) is a two-stage model involving the partial melting of lower crust, which mixes with fractionates of basaltic (possibly plume related) underplate to produce andesitic–dacitic magma. The intermediate-silicic melts migrate to upper crustal magma chambers via dyke emplacement where they undergo assimilation and fractional crystallization (AFC) before eruption as rhyolite. The actual composition of the primary basaltic underplate has previously not been possible to determine, given the near-absence of erupted basaltic material. However, the Sweeney Formation basalts, which have Mg numbers of ~ 65, and Cr and Ni contents of ~ 400 and ~ 200, respectively, could represent approximate compositions of the basaltic underplate, although they are not judged to be primitive melts.

An AFC-only model (Fig. 15) for the Mount Poster Formation rhyolites employing the Sweeney Formation basalts as a basaltic end-member and Palmer Land

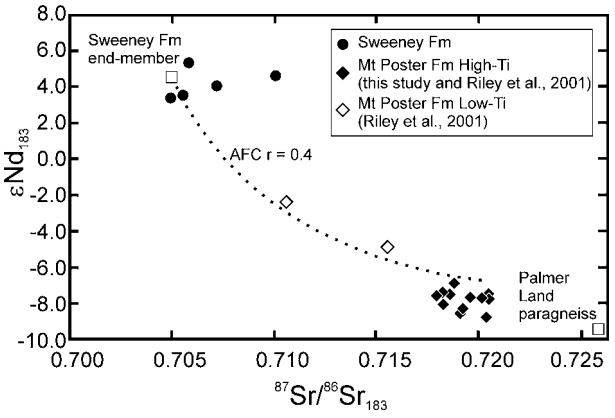

Figure 15. εNd_{183} v. $^{87}Sr/^{86}Sr_{183}$ plot for Mount Poster and Sweeney formation volcanic rocks. The dotted line is an assimilation fractional crystallization (AFC) curve between an average Sweeney Formation basalt, representing the mafic underplate ($^{87}Sr/^{86}Sr = 0.7049$; Sr = 120 ppm; $\varepsilon Nd = 4.5$; Nd = 9 ppm) and the crustal end-member, Palmer Land paragneiss (Wever, Millar & Pankhurst, 1994), ($^{87}Sr/^{86}Sr = 0.7260$; Sr = 175 ppm; $\varepsilon Nd_i = 9.75$; Nd = 45 ppm). DSr = 0.5, DNd = 0.1 and r = 0.4.

https://doi.org/10.1017/S0016756806002597 Published online by Cambridge University Press

paragneiss (Wever, Millar & Pankhurst, 1994) as a potential crustal contaminant (Riley *et al.* 2001) provides a plausible model for the composition of the high (intracaldera)- and low (extracaldera)-Ti rhyolites. Although the AFC model demonstrates that the two end-members were clearly important in the petrogenesis of the rhyolites, the more complex two-stage model of Riley *et al.* (2001) using the 'MASH' end-member provides a more satisfactory solution.

5. Summary and volcanic evolution model

The newly defined Ellsworth Land Volcanic Group includes the newly defined Sweeney Formation and the revised Mount Poster Formation. The intracaldera setting for the Mount Poster Formation is the dominant geological feature, with the rhyolites presumably sourced from several centres, which may have resulted in a sequence of overlapping or nested calderas forming the present-day elongate outcrop pattern. The basaltic and sedimentary rocks of the Sweeney Formation would have been emplaced outside the main caldera succession in a terrestrial environment, characterized by lakes and conifers.

Rowley, Schmidt & Williams (1982) defined the Mount Poster Formation as a 'sequence of volcanic rocks and sparse sedimentary rocks', the latter being subaerial fluvial or lacustrine. No lacustrine facies are found within the sediments of the Latady Basin in eastern Ellsworth Land (Hunter & Cantrill, 2006, this issue), apart from those associated with basaltic lava in the Sweeney Formation. Although Rowley, Schmidt & Williams (1982) make no mention of any basaltic material at Mount Poster they do stress that the majority of the Latady Basin is marine, and we believe that the interbedded terrestrial sediments they describe are lateral equivalents of the Sweeney Formation as described above.

Thin, outflow ignimbrite sheets occasionally occur outside the main caldera succession and are associated with the Sweeney Formation basaltic–sedimentary succession, indicating that the Mount Poster and Sweeney formations were coeval.

The Mount Poster Formation rhyolites have previously been grouped as part of the much wider Chon Aike Province of Patagonia and the Antarctic Peninsula (Pankhurst *et al.* 1998). The Chon Aike Province is a silicic large igneous province (Bryan *et al.* 2002) and is characterized by the near-absence of basaltic volcanism. Minor amounts of mafic (mostly basaltic andesite) volcanic rocks do occur in Patagonia (Pankhurst & Rapela, 1995), eastern Graham Land (Riley *et al.* 2003) and the Black Coast (Storey *et al.* 1987; Wever & Storey, 1992), but coeval basaltic rocks are essentially absent.

The near-absence of basaltic rocks during the main phase of silicic activity at *c.* 170 Ma (Pankhurst *et al.* 2000) is explained by the petrogenetic model of Riley *et al.* (2001) that describes the development of an impermeable rhyolite trap at the base of the continental crust, which prevents the migration of basaltic melts to the surface. This impermeable trap would develop following the basaltic underplating associated with the arrival of a mantle plume (perhaps as early as 190 Ma: Riley *et al.* 2005), therefore any basaltic melt escaping to the surface would be more likely to occur early in the history of the province.

Acknowledgements. This paper has benefited from the helpful comments of Bob Pankhurst and an anonymous reviewer. Martin Whitehouse and the staff at NORDSIM are thanked for their support, and we are grateful to financial support of the HI-LAT project. Chris Ottley (University of Durham) supplied the ICP-MS analyses and Dave Emley (University of Keele) carried out the XRF analyses. The field and air operations staff at Rothera Base are thanked for their support. This paper is NORDSIM publication no. 154.

References

BACON, C. R., FOSTER, H. L. & SMITH, J. G. 1990. Rhyolitic calderas of the Yukon-Tanana Terrane, east central Alaska – volcanic remnants of a mid-Cretaceous magmatic arc. *Journal of Geophysical Research* **95**, 21451–61.

BRYAN, S. E., RILEY, T. R., JERRAM, D. A., STEPHENS, C. J. & LEAT, P. T. 2002. Silicic volcanism: an undervalued component of large igneous provinces/volcanic rifted margins. In *Volcanic Rifted Margins* (eds M. A. Menzies, S. L. Klemperer, C. J. Ebinger and J. A. Baker), pp. 97–118. Boulder, Colorado: Geological Society of America, Special Paper no. 363.

CANTRILL, D. J. 2000. A Cretaceous macroflora from a freshwater lake deposit, President Head, Snow Island, Antarctica. *Palaeontographica Abteilung B* **253**, 153–91.

CANTRILL, D. J. & HUNTER, M. A. 2005. Macrofossil floras of the Latady Basin, Antarctic Peninsula. *New Zealand Journal of Geology and Geophysics* **48**, 537–53.

FANNING, C. M. & LAUDON, T. S. 1999. Mesozoic volcanism, plutonism and sedimentation in eastern Ellsworth land, West Antarctic. In *8th International symposium on Antarctic Earth Sciences, programme and abstracts* (ed. D. N. B. Skinner), p. 102. Victoria University of Wellington, New Zealand.

FLOWERDEW, M. J., MILLAR, I. L., HORSTWOOD, M. S. A., FANNING, C. M. & WHITEHOUSE, M. J. 2004. Utilizing in-situ measurement of Hf isotopes in zircon provenance studies. *32nd International Geological Congress, Florence, Italy, 2004. Programme with abstracts*, p. 1094.

FLOYD, P. A. 1986. Petrology and geochemistry of intraplate sheet-flow basalts, Nauru Basin, Deep Sea Drilling Project leg 89. In *Initial Reports of the Deep Sea Drilling Project, vol. 89* (eds R. Moberley and S. O. Schlanger), pp. 471–97. College Station, TX.

GEE, C. T. 1989. Permian *Glossopteris* and (Jurassic) *Elatocladus* megafossil floras from the English Coast, eastern Ellsworth Land, Antarctica. *Antarctic Science* **1**, 35–44.

HUNTER, M. A. & CANTRILL, D. J. 2006. A new stratigraphy for the Latady Basin, Antarctic Peninsula: Part 2. Latady

Group and basin evolution. *Geological Magazine* **143**, 797–819.

HUNTER, M. A., CANTRILL, D. J., FLOWERDEW, M. J. & MILLAR, I. L. 2005. Middle Jurassic age for the Botany Bay Group: implications for Weddell Sea Basin creation and southern hemisphere biostratigraphy. *Journal of the Geological Society, London* **162**, 745–8.

HUNTER, M. A., RILEY, T. R. & MILLAR, I. L. 2004. Middle Jurassic air fall tuff in the sedimentary Latady Formation, eastern Ellsworth Land: implications for the age of the Mount Poster Formation. *Antarctic Science* **16**, 185–90.

LAUDON, T. S. 1991. Petrology of sedimentary rocks from the English Coast, eastern Ellsworth Land. In *Geological evolution of Antarctica* (eds M. R. A.Thomson, J. A. Crame and J. W. Thomson), pp. 455–60. Cambridge: Cambridge University Press.

LAUDON, T. S. & FANNING, C. M. 2003. SHRIMP U–Pb age characteristics of detrital and magmatic zircons, eastern Ellsworth Land. In *9th International Symposium on Antarctic Earth Sciences, Antarctic contributions to global Earth Sciences, Potsdam, Germany. Programme and Abstracts*, 200–2.

LAUDON, T. S., THOMSON, M. R. A., WILLIAMS, P. L., MILLIKEN, K. L., ROWLEY, P. D. & BOYLES, J. M. 1983. The Jurassic Latady Formation, southern Antarctic Peninsula. In *Antarctic Earth Science* (eds R. L. Oliver, P. R. James and J. B. Jago), pp. 308–14. Cambridge: Cambridge University Press.

LEAT, P. T., RILEY, T. R., WAREHAM, C. D., MILLAR, I. L., KELLEY, S. P. & STOREY, B. C. 2002. Tectonic setting of primitive magmas in volcanic arcs: an example from the Antarctic Peninsula. *Journal of the Geological Society, London* **159**, 31–44.

LIPMAN, P. W. 1984. The roots of ash-flow calderas in western North America: windows into the tops of granitic batholiths. *Journal of Geophysical Research* **89**, 8801–41.

LUDWIG, K. R. 1998. On the treatment of concordant U–Pb ages. *Geochimica et Cosmochimica Acta* **62**, 665–76.

LUDWIG, K. R. 1999. Using Isoplot/Ex version 2, a geochronological toolkit for microsoft excel. *Berkeley Geochronological Special Publications* **1a**, 1–47.

MILLAR, I. L., PANKHURST, R. J. & FANNING, C. M. 2002. Basement chronology and the Antarctic Peninsula: recurrent magmatism and anatexis in the Palaeozoic Gondwana Margin. *Journal of the Geological Society, London* **159**, 145–58.

MILLAR, I. L., VAUGHAN, A. P. M., HORSTWOOD, M. S. A., FLOWERDEW, M. J., PANKHURST, R. J., PASHLEY, V. H. & FANNING, C. M. 2003. Hf isotopes in detrital zircons from accretionary complex rocks of Alexander Island, Antarctic Peninsula. EGS–AGU–EUG Joint Assembly, Nice, France. *Geophysical Research Abstracts* **5**, 10003.

MILLAR, I. L., WILLAN, R. C. R., WAREHAM, C. D. & BOYCE, A. J. 2001. The role of crustal and mantle sources in the genesis of granitoids of the Antartctic Peninsula and adjacent crustal blocks. *Journal of the Geological Society, London* **158**, 855–68.

NAKAMURA, N. 1974. Determination of REE, Ba, Fe, Mg, Na and K in carbonaceous and ordinary chondrites. *Geochimica et Cosmochimica Acta* **38**, 757–73.

PANKHURST, R. J., LEAT, P. T., SRUOGA, P., RAPELA, C. W., MÁRQUEZ, M., STOREY, B. C. & RILEY, T. R. 1998. The Chon Aike silicic igneous province of Patagonia and related rocks in Antarctica: a silicic large igneous province. *Journal of Volcanology and Geothermal Research* **81**, 113–36.

PANKHURST, R. J. & RAPELA, C. R. 1995. Production of Jurassic rhyolites by anatexis of the lower crust of Patagonia. *Earth and Planetary Science Letters* **134**, 23–36.

PANKHURST, R. J., RILEY, T. R., FANNING, C. M. & KELLEY, S. P. 2000. Episodic silicic volcanism in Patagonia and the Antarctic Peninsula: chronology of magmatism associated with break-up of Gondwana. *Journal of Petrology* **41**, 605–25.

PEARCE, J. A., BAKER, P. E., HARVEY, P. K. & LUFF, I. W. 1995. Geochemical evidence for subduction fluxes, mantle melting and fractional crystallisation beneath the South Sandwich island arc. *Journal of Petrology* **36**, 1073–1109.

PEARCE, J. A. & PEATE, D. W. 1995. Tectonic implications of the composition of volcanic arc magmas. *Annual Reviews in Earth and Planetary Science* **23**, 251–85.

QUILTY, P. G. 1972. Middle Jurassic brachiopods from Ellsworth Land, Antarctica. *New Zealand Journal of Geology and Geophysics* **15**, 140–7.

QUILTY, P. G. 1977. Late Jurassic bivalves from Ellsworth Land, Antarctica; their systematics and palaeobiogeographic implications. *New Zealand Journal of Geology and Geophysics* **20**, 1033–80.

QUILTY, P. G. 1983. Bajocian bivalves from Ellsworth Land, Antarctica. *New Zealand Journal of Geology and Geophysics* **26**, 395–418.

REES, P. M. & CLEAL, C. J. 2004. Early Jurassic floras from Hope Bay and Botany Bay, Antarctica. *Special Papers in Palaeontology* **72**, 1–90.

RILEY, T. R. & KNIGHT, K. B. 2001. Age of pre-break-up Gondwana magmatism. *Antarctic Science* **13**, 99–110.

RILEY, T. R. & LEAT, P. T. 1999. Large volume silicic volcanism along the proto-Pacific margin of Gondwana: lithological and stratigraphical investigations from the Antarctic Peninsula. *Geological Magazine* **136**, 1–16.

RILEY, T. R., LEAT, P. T., CURTIS, M. L., MILLAR, I. L., DUNCAN, R. A. & FAZEL, A. 2005. Early–Middle Jurassic Dolerite Dykes from Western Dronning Maud Land (Antarctica): Identifying Mantle Sources in the Karoo Large Igneous Province. *Journal of Petrology* **46**, 1489–1524.

RILEY, T. R., LEAT, P. T., KELLEY, S. P., MILLAR, I. L. & THIRLWALL, M. F. 2003. Thinning of the Antarctic Peninsula lithosphere through the Mesozoic: evidence from Middle Jurassic basaltic lavas. *Lithos* **67**, 163–79.

RILEY, T. R., LEAT, P. T., PANKHURST, R. J. & HARRIS, C. 2001. Origins of large volume rhyolitic volcanism in the Antarctic Peninsula and Patagonia by crustal melting. *Journal of Petrology* **42**, 1043–65.

ROWLEY, P. D., SCHMIDT, D. L. & WILLIAMS, P. L. 1982. Mount Poster Formation, southern Antarctic Peninsula. Mount Poster Formation, southern Antarctic Peninsula and eastern Ellsworth Land. *Antarctic Journal of the United States* **17**, 38–9.

SCARROW, J. H., LEAT, P. T., WAREHAM, C. D. & MILLAR, I. L. 1998. Geochemistry of mafic dykes in the Antarctic Peninsula continental-margin batholith: a record of arc evolution. *Contributions to Mineralogy and Petrology* **131**, 289–305.

STACEY, J. S. & KRAMERS, J. D. 1975. Approximation of terrestrial lead isotope evolution by a two-stage

model. *Earth and Planetary Science Letters* **26**, 207–21.

STEIGER, R. H. & JÄGER, E. 1977. Subcommission on geochronology; convention on the use of decay constants in geo- and cosmochronology. *Earth and Planetary Science Letters* **36**, 359–62.

STOREY, B. C., ALABASTER, T., HOLE, M. J., PANKHURST, R. J. & WEVER, H. E. 1992. Role of subduction plate boundary forces during the initial stages of Gondwana break-up: evidence from the proto-Pacific margin of Antarctica. In *Magmatism and the causes of continental break-up* (eds B. C. Storey, T. Alabaster and R. J. Pankhurst), pp. 149–63. Geological Society of London, Special Publication no. 68.

STOREY, B. C. & GARRETT, S. W. 1985. Crustal growth of the Antarctic Peninsula by accretion, magmatism and extension. *Geological Magazine* **122**, 5–14.

STOREY, B. C., WEVER, H. E., ROWLEY, P. D. & FORD, A. B. 1987. Report on Antarctic fieldwork: the geology of the central Black Coast, eastern Palmer Land. *British Antarctic Survey Bulletin* **77**, 145–55.

THOMSON, M. R. A. 1983. Late Jurassic ammonites from the Orville Coast, Antarctica. In *Antarctic Earth Science* (eds R. L. Oliver, P. R. James and J. B. Jago), pp. 315–19. Cambridge University Press.

THOMSON, M. R. A. & PANKHURST, R. J. 1983. Age of post-Gondwanian calc-alkaline volcanism in the Antarctic Peninsula region. In *Antarctic Earth Science* (eds R. L. Oliver, P. R. James and J. B. Jago), pp. 328–33. Cambridge University Press.

WEVER, H. E., MILLAR, I. L. & PANKHURST, R. J. 1994. Geochronology and radiogenic isotope geology of Mesozoic rocks from eastern Palmer Land, Antarctic Peninsula: crustal anatexis in arc-related granitoid genesis. *Journal of South American Earth Sciences* **7**, 69–83.

WEVER, H. E. & STOREY, B. C. 1992. Bimodal magmatism in northeast Palmer Land, Antarctic Peninsula: geochemical evidence for a Jurassic ensialic back-arc basin. *Tectonophysics* **205**, 239–59.

WHITEHOUSE, M. J., CLAESSON, S., SUNDE, T. & VESTIN, J. 1997. Ion microprobe geochronology and correlation of Archaean gneisses from the Lewisian Complex of Gruinard Bay, northwestern Scotland. *Geochimica et Cosmochimica Acta* **61**, 4429–38.

WHITEHOUSE, M. J., KAMBER, B. & MOORBATH, S. 1999. Age significance of U–Th–Pb zircon data from early Archaean rocks of west Greenland – a reassessment based on combined ion-microprobe and imaging studies. *Chemical Geology* **160**, 201–24.

WIEDENBECK, M., ALLÉ, P., CORFU, F., GRIFFIN, W. L., MEIER, M., OBERLI, F., VON QUADT, A., RODDICK, J. C. & SPIEGEL, W. 1995. Three natural zircon standards for U–Th–Pb, Lu–Hf, trace element and REE analysis. *Geostandards Newsletter* **19**, 1–23.

WILLIAMS, P. L., SCHMIDT, D. L., PLUMMER, C. C. & BROWN, L. E. 1972. Geology of the Lassiter Coast area, Antarctic Peninsula: Preliminary Report. In *Antarctic Geology and Geophysics* (ed. R. J. Adie), pp. 143–53. Oslo: Universitetsforlaget.